RESEARCH ARTICLE

Enhanced Chaotic Manta Ray Foraging Algorithm for Function Optimization and Optimal Wind Farm Layout Problem

FATIMA DAQAQ[1,2], RACHID ELLAIA[2], MOHAMMED OUASSAID[1], (Senior Member, IEEE), HOSSAM M. ZAWBAA[3,4], AND SALAH KAMEL[5]

[1]Engineering for Smart and Sustainable Systems Research Center, Mohammadia School of Engineers, Mohammed V University in Rabat, Rabat 10090, Morocco
[2]Laboratory of Study and Research for Applied Mathematics, Mohammadia School of Engineers, Mohammed V University in Rabat, Rabat 10090, Morocco
[3]Faculty of Computers and Artificial Intelligence, Beni-Suef University, Beni-Suef 62511, Egypt
[4]CeADAR Irelands Center for Applied AI, Technological University Dublin, Dublin, D07 EWV4 Ireland
[5]Electrical Engineering Department, Faculty of Engineering, Aswan University, Aswan 81542, Egypt

Corresponding authors: Hossam M. Zawbaa (hossam.zawbaa@gmail.com) and Fatima Daqaq (fati.daqaq@gmail.com)

ABSTRACT Manta ray foraging optimization (MRFO) algorithm is relatively a novel bio-inspired optimization technique directed to given real-world engineering problems. In this present work, wind turbines layout (WTs) inside a wind farm is considered a real nonlinear optimization problem. In spite of the better convergence of MRFO, it gets stuck into local optima for large problems. The chaotic sequences are among the performed techniques used to tackle this shortcoming and improve the global search ability. Therefore, ten chaotic maps have been embedded into MRFO. To affirm the performance of the suggested chaotic approach CMRFO, it was first assessed using the IEEE CEC-2017 benchmark functions. This examination has been systematically compared to eight well-known optimization algorithms and the original MRFO. The non-parametric Wilcoxon statistical analysis significantly demonstrates the superiority of CMRFO as it ranks first in most test suites. Secondly, the MRFO and its best enhanced chaotic version were tested on the complex problem of finding the optimal locations of wind turbines within a wind farm. Besides, the application of the CMRFO to the wind farm layout optimization (WFLO) problem aims to minimize the cost per unit power output and increase the wind-farm efficiency and the electrical power engendered by all WTs. Two representative scenarios of the problem have been dealt with a square-shaped farm installed on an area of 2 km × 2 km, including variable wind direction with steady wind speed, and both wind direction and speed are variable. The WFLO outcomes reveal the CMRFO capability to find the optimal locations of WTs, which generates a maximum power for the minimum cost compared to three stochastic approaches and other previous studies. At last, the suggested CMRFO with Singer chaotic sequence has been successfully enhanced by accelerating the convergence and providing better accuracy to find the global optimum.

INDEX TERMS Chaotic sequences, manta ray foraging optimization, stochastic optimization, wake effect, wind farm layout, wind turbines.

NOMENCLATURE

a	Axial induction factor.
ABC	Artificial bee colony.
AOA	Arithmetic optimization algorithm.
BWOA	Black widow optimization algorithm.
C	Chaotic variables.
CEC-2017	Congress on evolutionary computation 2017.
CMRFO	Chaotic manta ray foraging optimization.
d	Dimension of the problem.

D	Rotor diameter.
DDOA	Dynamic differential annealed optimization.
α	Entrainment constant.
h	Hub height.
HHO	Harris hawks optimization.
Lb	Lower bound.
LFD	Levy flight distribution.
MRFO	Manta ray foraging optimization.
N	Population size.
r	Rotor radius.
r_1	Downstream rotor radius.
r_2	Wake region radius.
SCA	Sine cosine algorithm.
SSA	Salp swarm algorithm.
T	Maximum iteration.
Ub	Upper bound.
u_∞	Free incident wind speed.
WFLO	Wind farm layout optimization.
WTs	Wind turbines.

I. INTRODUCTION

The development of renewable energy is a priority of the worldwide energy strategy marked by reducing electrical power output costs. Besides, renewable energy plays an important role in future necessities by keeping a clean, safe and better environment, and that is why often denoted as clean energy or green energy. Generally, solar, wind, biomass, hydroelectric, and geothermal power are all referred to as clean sources. Over the last two decades, wind energy has increasingly received worldwide attention among other various kinds of energies and has become an important power source. The global world wind energy installed capacity was 539.1 GW at the end of 2017 and is predicted to achieve 840 GW by 2022 [1]. Generally, in the field of renewable energy, wind power is usually produced by wind turbines that convert kinetic energy into electrical power. Therefore, one of the techniques used to raise the rate of wind power production is to improve wind farm planning by optimizing the placement of wind turbines in a wind park.

As wind farm layout optimization is a complicated task, many extensive efforts have been addressed using metaheuristic optimization algorithms to maximize the energy output and efficiency at a minimum cost per unit. It is worth noting that the first optimization approach used for the WFLO problem is outlined in the work of Mosetti *et al.* in 1994 [2]. They employed the wake model developed by Jensen [3]. This approach is called a genetic algorithm; it extracts a maximum output power at a minimum cost per unit value. For the same algorithm applied by Mosetti, several works employed GA and its variants [4]–[12]. Referring to [13], the authors attempted to solve the power produced by a wind farm using the particle swarm optimization approach (PSO). This last was developed by many researchers in order to find the improved layout of the wind farm as demonstrated in [14] – [18]. The main objectives of all these studies are

focused on enhancing the power output in wind farm layouts. In this regard, more computation intelligence approaches have been improved and introduced to solve this problem such as: evolutionary algorithm (EA) [19], monte carlo simulation [20], greedy algorithm [21], simulated annealing (SA) [22], sequential convex programming [23], random search algorithm (RSA) [24]–[27], multi-objective random search algorithm (MORSA) [28], ant colony (AC) [29], ant lion optimization (ALO) [30], sparrow search algorithm (SSA) [31], single-objective hybrid optimizer (SOHO) [32], binary invasive weed optimization (BIWO) [33], [34]; differential evolution(DE) [35], Jaya algorithm [36], integer programming [37], success history based adaptive differential evolution (L-SHADE) [38], cuckoo search (CS) [39], [40]; biogeography-based optimization (BBO) [41], multi-team perturbation-guiding jaya (MTPG-Jaya) [42], water cycle optimization (WCO) [43], dynastic optimization algorithm (DOA) [44], binary most valuable player algorithm (BMVPA) [45], adaptive neuro-fuzzy inference system (ANFIS) [46], extended pattern search algorithm (EPS) [47].

In this present study, the optimal wind turbine layout was for the first time performed based on a modified new inspired evolutionary algorithm recently developed in 2020 by Zhao *et al.* [48]; named manta ray foraging optimization (MRFO). In that respect, many previous pieces of research focused on the application of MRFO and its variants in numerous research areas, including electrical engineering. For instance, the authors in [49] have examined the global maximum power point (GMPP) of partially shaded MJSC PV array applying the MRFO algorithm. In addition, fahd *et al.* [50] applied the standard MRFO to perform the dynamic operation for connecting PV into the grid system. Regarding the work of Selem *et al.* [51], the MRFO was applied to define the unknown electrical parameters of proton exchange membrane fuel cells (PEMFC) stacks, which is considered a constrained optimization problem. El-Hameed *et al.* [52] used MRFO to solve the solar module parameters identifications of three diode equivalent models (3DeM). In the field of speech emotion feature selection, Chattopadhyay *et al.* [53] utilized MRFO to recognize emotion from speech signals in order to select the reliable features for classification and discard the redundant ones. Besides, in an attempt to ameliorate the performance of the suggested approach, Dalia *et al.* [54] introduced a modified MRFO by using fractional-order optimization algorithms in order to enhance its exploitation ability. Furthermore, another alteration occurred by merging MRFO with the simulated annealing algorithm (SA) to tune the parameters for the proportional-integral-derivative (PID) controller. In their work, the SA was integrated as the initial population of MRFO with the aim of raising its convergence speed [55]. Referring to [56], a binary version of MRFO has been proposed using four S-Shaped and four V-Shaped transfer functions for the feature selection problem. In the bio-medical area, Karrupusamy utilized a hybrid MRFO to identify the issue in existing brain tumors by using a convolutional neural
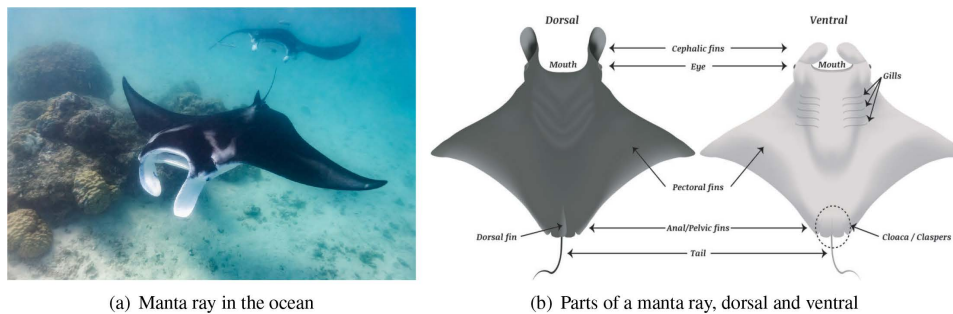
(a) Manta ray in the ocean

(b) Parts of a manta ray, dorsal and ventral

FIGURE 1. **Manta ray body form.**

network as a classifier that classifies the features and supplies optimal classification results [57]. Within the scope of COVID-19, a hybrid MRFO with differential evolution (DE) was employed as a methodology for diagnosing the disease based on the lungs x-ray images of the potential patients [58]. As opposed to the single optimization algorithm, a multi-objective manta ray foraging optimization (MO-MRFO) based weighted sum was utilized to perform the allocation and size of distributed generations (DG) [59]. In their work, the objective functions were converted to a single objective optimization problem using the weighted factors. In this sense, Shaheen *et al.* have applied MO-MRFO to handle the OPF problem for hybrid AC and multi-terminal direct current (MTDC) power grids [60]. Additionally, in an effort to resolve the optimal power flow incorporating wind/solar/small-hydro power, a multi-objective version of MRFO is suggested in [61].

Along these lines, the significant powerful features of MRFO and its borrowed evolutionary algorithms mentioned above, motivated us to improve a novel variant of MRFO based on chaos sequences, named chaotic manta ray foraging optimization (CMRFO), for solving the complex wind farm layout design issue. However, no research in the literature extends the MRFO algorithm to deal with the WFLO problem. Besides, it is widely known that combining the meta-heuristic methods with chaotic maps increases the algorithms' performance and convergence speed. It is seen from the literature review that there are many works which used chaotic maps such as, chaotic grasshopper optimization algorithm (GOA) [62], bat algorithm (BA) [63], bird swarm algorithm (BSA) [64], crow search algorithm (CSA) [65], genetic algorithm (GA) [66], big bang–big crunch algorithm (BB–BC) [67], krill herd algorithm (KHA) [68], artificial immune system optimization algorithm (AIS) [69], atom search optimization (ASO) [70], dragonfly algorithm (DA) [71], and gravitational search algorithm (GSA) [72], harmony search algorithm (HSA) [73], imperialist competitive algorithm (ICA) [74], grey wolf optimization (GWO) [75], particle swarm optimization (PSO) [76], moth-flame optimization (MFO) [77], salp swarm algorithm (SSA) [78], symbiotic organisms search algorithm (SOS) [79], cuckoo search algorithm (CSA) [80], electromagnetic field optimization (EFO) [81], biogeography-based optimization (BBO) [82], etc.

The principal contributions of this current paper can be summarized as follows:
- A selected of ten different chaotic maps have been integrated into MRFO.
- A set of twenty-nine benchmark problems of CEC-2017 is implemented to show the performance of CMRFO, including composite, hybrid, multimodal and unimodal functions.
- The best chaotic sequence is applied to the WFLO problem for the first time.
- The suggested approach is compared with the standard MRFO and other existing stochastic algorithms.

The remaining parts of this work are structured as follows: Section II introduces the fundamental mathematical formulations of the WFLO problem, including the wind turbine, wind farm, wake model, power product and cost per unit. A brief description of MRFO is provided in Section III, besides the concepts, steps and implementation of chaotic MRFO. Section IV deals with the experiments conducted in this current study. In closing, Section V concludes the study with a conclusion and a discussion of the future work of MRFO.

II. OPTIMIZATION METHODOLOGY

A. MANTA RAY FORAGING OPTIMIZATION (MRFO)

As its name signifies, the MRFO is a bio-inspired algorithm simulating the feeding behavior of manta ray marine creatures [83]. Their cephalic fin movements and body turns to make them as elegant marine critters; they swim as birds freely fly. In spite of the colossal statue of these fascinating creatures, they feed on some tiny organisms (planktons) living in the sea; accordingly, they are considered the gentle giants of the sea [84]. According to their species, Manta rays can survive in tropical, subtropical and temperate oceans. Therefore, there are two species of manta ray in nature, the giant manta ray and the reef manta. The first kind is called Mantas birostris; they are considered the giant of the two oceanic species; they can reach up to 9 m in width and have a dark color around the mouth. On the other side, Mantas alfredi is the resident in reef manta, reaching a width up to 4.5 m. The shape of a manta ray is illustrated in Fig.1. Generally, depending on the number of mantas and their swimming behavior, there are eight intelligent manta foraging strategies: chain, cyclone, somersault, surface,
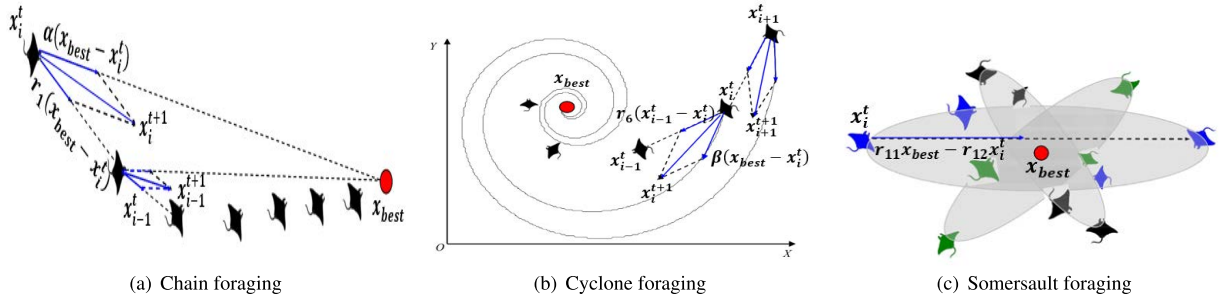
(a) Chain foraging **(b) Cyclone foraging** **(c) Somersault foraging**

FIGURE 2. Simulation model of manta ray foraging behaviors.

sideways, piggy-back, straight, and bottom feedings [85]. In terms of MRF optimization, three main mechanisms were addressed: chain, somersault, and cyclone feeding. Fig. 2. illustrates these three foraging behaviors [48]. Furthermore, the manta rays are assumed to search agents which explore the planktons' location and proceed towards them. Then the planktons at significant concentration represent the best solution.

In the manner of the population-based optimization algorithms, MRFO is first initialized by a random process as introduced in below [48]:

$$x_i = \text{Lb}_i + \text{rand} \times (\text{Ub}_i - \text{Lb}_i), \ i = 1, 2, \dots, N \quad (1)$$

where Ub and Lb are the maximum and minimum bounds of variables in the search space, rand is a random number between 0 and 1, and rand $\in [0,1]$.

The details of the three main behaviors are explicated and mathematically modeled in the following subsections.

1) CHAIN FORAGING
In chain feeding, the mantas foraging in the group, forming a line of dozen individuals lining up head-to-tail in horizontal movement with a fully open mouth. The female manta rays piggyback the smaller males in order to match the beating of the female's pectoral fins. The manta chain is divided into the leader, which is the manta at the front of the chain, and the followers. Therefore, the missed planktons by the previous manta rays will be consumed by the next ones. During the feeding process, each individual updates its position towards the best plankton source and towards the manta ray in front of the current individual until it reaches the best position. The following equations represent the position updating equations [48]:

$$x_{i,j}^{t+1} = \begin{cases} x_{i,j}^t + r_1 \left(x_{\text{best},j}^t - x_{i,j}^t \right) \\ + \alpha \left(x_{\text{best},j}^t - x_{i,j}^t \right), & i = 1 \\ x_{i,j}^t + r_2 \left(x_{i-1,j}^t - x_{i,j}^t \right) \\ + \alpha \left(x_{\text{best},j}^t - x_{i,j}^t \right), & i = 2, \dots, N \end{cases} \quad (2)$$

where $x_{i,j}$ is the position of ith manta ray in j^{th} dimension, r_1 and r_2 are the random vector in range [0-1], $x_{\text{best},j}^t$ is the best plankton concentration position, α is a weight coefficient that

is expressed as [48]:

$$\alpha = 2r_3 \sqrt{|\log(r_4)|} \quad (3)$$

where r_3 and r_4 introduce the random vector in range [0-1].

2) CYCLONE FORAGING
This attitude was observed in manta alfredi species. It seems to be the previous feeding strategy, except that the chain moves in a spiral shape after the mantas find out the high concentration site of plankton. Along with this spiral behavior, each manta swims toward the one in front of it.

This spiral movement is mathematically formulated as [48]:

$$x_{i,j}^{t+1} = \begin{cases} x_{\text{best},j} + r_5 \left(x_{\text{best},j}^t - x_{i,j}^t \right) \\ + \beta \left(x_{\text{best},j}^t - x_{i,j}^t \right), & i = 1 \\ x_{\text{best},j} + r_6 \left(x_{i-1,j}^t - x_{i,j}^t \right) \\ + \beta \left(x_{\text{best},j}^t - x_{i,j}^t \right), & i = 2, \dots, N \end{cases} \quad (4)$$

where r_5 and r_6 present the random value in [0-1], β is the weight coefficient that is formulated as [48]:

$$\beta = 2e^{r_7 \frac{T-t+1}{T}} \sin(2\pi r_7) \quad (5)$$

where r_7 denotes the random vector in range [0-1], T and t are the maximum and current iteration, respectively.

In the field of searching mechanisms, cyclone foraging possesses improved intensification and diversification processes. The exploitation potential increases based on the best plankton region found as mantas reference positions. In addition, the cyclone behavior boosts the exploration process by enforcing each manta to update its position to a new random one that is far away from the current best position. This exploration phase incites the MRFO algorithm to achieve the overall optimal solution in accordance with the mathematical equations described below [48]:

$$x_{\text{rand},j} = \text{Lb}_j + r_8 \left(\text{Ub}_j - \text{Lb}_j \right) \quad (6)$$

$$x_{i,j}^{t+1} = \begin{cases} x_{\text{rand},j} + r_9 \left(x_{\text{rand},j} - x_{i,j}^t \right) \\ + \beta \left(x_{\text{rand},j} - x_{i,j}^t \right), & i = 1 \\ x_{\text{rand},j} + r_{10} \left(x_{i-1,j}^t - x_{ij}^t \right) \\ + \beta \left(x_{\text{rand},j} - x_{i,j}^t \right), & i = 2, \dots, N \end{cases} \quad (7)$$

Algorithm 1 Manta Ray Foraging Optimization

1: **Function** $x = \text{MRFO}(N, T, f(x), \text{Ub}, \text{Lb}, d)$
2: Generate a uniform random initial population of mantas x respect to Ub and Lb using:
3: $x_i = \text{Lb}_i + \text{rand} \times (\text{Ub}_i - \text{Lb}_i), \quad i = 1, 2, \ldots, N$
4: Compute the fitness function of each manta
5: Find the best solution x_{best} which is the plankton with high concentration in the initial population
6: **while** $t < T$ (stopping criteria) **do**
7:     **for** $i = 1 : N$ (each manta in the population) **do**
8:         **if** rand(0, 1) < 0.5 **then**
9:             %%Cyclone foraging
10:             **if** $t/T < \text{rand}(0,1)$ **then**
11:                 Update the mantas' position using (6) and (7)
12:             **else**
13:                 Update the mantas' position using (4)
14:             **end if**
15:         **else**
16:             %%Chain foraging
17:             Update the mantas' position using (2)
18:         **end if**
19:         Evaluate new solution of each manta $f\left(x_i^{t+1}\right)$
20:         **if** new solutions are better, $f\left(x_i^{t+1}\right) < f\left(x_{\text{best}}\right)$ **then**
21:             Update them in the population, $x_{\text{best}} = x_i^{t+1}$
22:         **end if**
23:     **end for**
24:     %%Somersault foraging
25:     **for** $i = 1 : N$ (each manta in the population) **do**
26:         Update the mantas' position using (8)
27:         Evaluate new solution of each manta $f\left(x_i^{t+1}\right)$
28:         **if** new solutions are better, $f\left(x_i^{t+1}\right) < f\left(x_{\text{best}}\right)$ **then**
29:             Update them in the population, $x_{\text{best}} = x_i^{t+1}$
30:         **end if**
31:     **end for**
32: **end while**
33: Output the best solution found

---

where $x_{\text{rand},j}$ is the random position generated inside the search space.

3) SOMERSAULT FORAGING

As a final behavior, each manta feeds individually by somersaulting around itself, which increase the plankton intake considering a common pivot point for all manta bunch. Then, each individual updates their position around the pivot. The mathematical equation of somersault feeding is given as follows [48]:

$$x_{i,j}^{t+1} = x_{i,j}^t + S\left(r_{11} x_{\text{best},j} - r_{12} x_{i,j}^t\right), \quad i = 1, 2, \ldots, N \quad (8)$$

where r_{11}, r_{12} depict the random values between 0 and 1. S is the somersault factor, $S = 2$.

MRFO's diversification and intensification phases are balanced using the value of the variations t/T, which is

gradually increasing. The expression $(t/T > \text{rand})$ denotes the exploration stage; reversibly, exploitation process is adopted. The main steps followed in MRFO are demonstrated in Algorithm 1.

B. CHAOTIC MANTA RAY FORAGING OPTIMIZATION (CMRFO)

1) CHAOTIC THEORY

Chaos is one of the universal mathematical phenomena. It appears in some nonlinear dynamical systems. In fact, these systems are characterized by a high sensitivity to their primary conditions, in which slight variations in the initial conditions can radically lead to significant outcomes after several cycles in the system. This effect is known as the butterfly effect, which was founded by Lorenz in 1963 [86]. Chaos refers to a deterministic random-like process. Although the system model is deterministic, its behavior
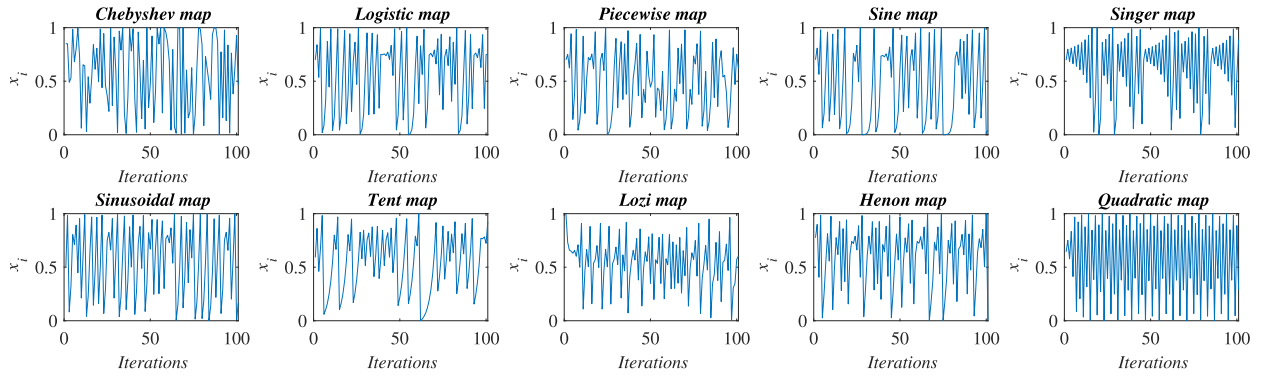
FIGURE 3. Visualization of chaotic maps.

TABLE 1. Descriptions of the Chaotic maps.

No	Maps names	Maps expressions	Ranges
CMRFO1	Chebyshev [88]	$x_{i+1} = \cos\left(i\cos^{-1}(x_i)\right)$	(-1,1)
CMRFO2	Logistic [89]	$x_{i+1} = ax_i(1 - x_i), \quad a = 4$	(0,1)
CMRFO3	Piecewise [82]	$x_{i+1} = \begin{cases} \frac{x_i}{P} & 0 \leq x_i \prec P \\ \frac{x_i - P}{0.5 - P} & P \leq x_i \prec 0.5 \\ \frac{1 - P - x_i}{0.5 - P} & 0.5 \leq x_i < 1 - P \\ \frac{1 - x_i}{P} & 1 - P \leq x_i \prec 1 \end{cases}$	(0,1)
CMRFO4	Sine [82]	$x_{i+1} = \frac{a}{4}\sin(\pi x_i), \quad a = 4$	(0,1)
CMRFO5	Singer [82]	$x_{i+1} = \mu\left(7.86x_i - 23.31x_i^2 + 28.75x_i^3 - 13.302875x_i^4\right), \quad \mu = 1.07$	(0,1)
CMRFO6	Sinusoidal [82]	$x_{i+1} = ax_i^2\sin(\pi x_i), \quad a = 2.3$	(0,1)
CMRFO7	Tent [90]	$x_{i+1} = \begin{cases} \frac{x_i}{0.7} & x_i \prec 0 \\ \frac{10}{3}(1 - x_i) & x_i \geq 0.7 \end{cases}$	(0,1)
CMRFO8	Lozi [91]	$y_{i+1} = 1 - 1.7\lvert y_i\rvert + x_i$ $x_{i+1} = 0.5y_i$	(-1,1)
CMRFO9	Henon [66]	$x_{i+1} = 1 - ax_i^2 + y_i, \quad a = 1.4$ $y_{i+1} = bx_i, \quad b = 0.3$	(0,1)
CMRFO10	Quadratic [92]	$x_{i+1} = a - x_i^2, \quad a = 1.4$	(0,1)

appears stochastic. This means that the future behavior of such systems is entirely determined by their initial chaotic variables, without any random variable being involved. The chaotic systems exhibit the following characteristics: non-linearity, ergodicity, determinism, hypersensitivity, unpredictability, and irregularity. The chaotic dynamical systems study can be formulated with a discrete function of dimension 1 as follows [87]:

$$x(k + 1) = f(x(k)), \quad x \in \mathbb{R}, \ k \in \mathbb{N}^* \tag{9}$$

Lately, chaos maps have been widely employed for adjusting the stochastic algorithm parameters, due to the fact that chaos often offers high searching behavior compared to stochastic variables.

2) DIFFERENT CHAOTIC SEQUENCES FOR MRFO

In this section, the chaotic maps employed for improving the MRFO are first presented, and then the steps followed for embedding them are described. Ten chaotic variants are considered in this article as: Chebyshev [88], Logistic [89], Piecewise [82], Sine [82], Singer [82], Sinusoidal [82], Tent [90], Lozi [91], Henon [66], Quadratic [92]. Furthermore, there are more maps have been used to improve the suggested approach but have not been presented due to the worst results found. The visualization of all chaotic maps

utilized is shown in Fig. 3. The mathematical formulations for all these chaotic variants are listed in Table 1, their ranges are shifted to be in the interval of (0,1) with an initial value of 0.7 ($x_0 = 0.7$).

It is widely known that in any nature-inspired optimization algorithm, there is always a scope for modifications, avoiding the premature convergences to escape from different local optima and exploring more accurate solutions. From this perspective, the chaos maps dynamical features were widely used to overcome these shortcomings, enhance the intensification and diversification processes, and appraise the performance of stochastic algorithms. For this purpose, using the chaotic mapping mechanism with the standard MRFO in both search strategies and speed parameters achieves its ability to find the global optimum for the complex high-dimensional problem. The chaotic manta ray foraging optimization CMRFO was generated by substituting random values in the basic MRFO with a chaotic variables, especially the random values r_1, r_2, r_5, r_6, r_8, and r_{11} as explained in Algorithm 2.

III. PROBLEM FORMULATION
In this section, the wind farm mathematical modeling will be discussed. Like the assumptions done in the previous works, the Jensen wake model [3] is considered in this study; in

---

Algorithm 2 Chaotic Manta Ray Foraging Optimization

1: **Function** x = CMRFO(N, T, $f(x)$, Ub, Lb, d, C)
2: Generate a uniform random initial population of mantas x respect to Ub and Lb using:
3: $x_i = \text{Lb}_i + \text{rand} \times (\text{Ub}_i - \text{Lb}_i)$, $i = 1, 2, \ldots, N$
4: Compute the fitness function of each manta
5: Find the best solution x_{best} which is the plankton with high concentration in the initial population
6: **while** $t < T$ (stopping criteria) **do**
7:     **for** $i = 1 : N$ (each manta in the population) **do**
8:         **if** rand(0, 1) < 0.5 **then**
9:             %%Cyclone foraging
10:             **if** $t/T < $ rand(0, 1) **then**
11:                 $x_{\text{rand}} = Lb + C(t)\,(Ub-Lb)$
12:                 $x_i^{t+1} = \begin{cases} x_{\text{rand}} + r_9\left(x_{\text{rand}} - x_i^t\right) + \beta\left(x_{\text{rand}} - x_i^t\right), & i = 1 \\ x_{\text{rand}} + r_{10}\left(x_{i-1}^t - x_i^t\right) + \beta\left(x_{\text{rand}} - x_i^t\right), & i = 2, \ldots, N \end{cases}$
13:             **else**
14:                 $x_i^{t+1} = \begin{cases} x_{\text{best}} + C(t)\left(x_{\text{best}} - x_i^t\right) + \beta\left(x_{\text{best}} - x_i^t\right), & i = 1 \\ x_{\text{best}} + C(t)\left(x_{i-1}^t - x_i^t\right) + \beta\left(x_{\text{best}} - x_i^t\right), & i = 2, \ldots, N \end{cases}$
15:             **end if**
16:         **else**
17:             %%Chain foraging
18:             $x_i^{t+1} = \begin{cases} x_i^t + C(t)\left(x_{\text{best}} - x_i^t\right) + \alpha\left(x_{\text{best}} - x_i^t\right), & i = 1 \\ x_i^t + C(t)\left(x_{i-1}^t - x_i^t\right) + \alpha\left(x_{\text{best}} - x_i^t\right), & i = 2, \ldots, N \end{cases}$
19:         **end if**
20:         Evaluate new solution of each manta $f\left(x_i^{t+1}\right)$
21:         **if** new solutions are better, $f\left(x_i^{t+1}\right) < f\left(x_{\text{best}}\right)$ **then**
22:             Update them in the population, $x_{\text{best}} = x_i^{t+1}$
23:         **end if**
24:     **end for**
25:     %%Somersault foraging
26:     **for** $i = 1 : N$ (each manta in the population) **do**
27:         $x_i^{t+1} = x_i^t + S\left(C(t)x_{\text{best}} - r_{12}x_i^t\right)$, $i = 1, 2, \ldots, N$
28:         Evaluate new solution of each manta $f\left(x_i^{t+1}\right)$
29:         **if** new solutions are better, $f\left(x_i^{t+1}\right) < f\left(x_{\text{best}}\right)$ **then**
30:             Update them in the population, $x_{\text{best}} = x_i^{t+1}$
31:         **end if**
32:     **end for**
33: **end while**
34: Output the best solution found

---

addition to a square-shaped wind farm area (2 km × 2 km) partitioned into 100 possible turbine positions, each cell dimension is taken to be 200 m × 200 m, and each wind turbine is installed at the center of each cell with a hub height of 60 m and a rotor diameter of 40 m. The wind farm grid model in use is presented in Fig. 4(a).

A. WAKE MODEL

As mentioned previously, the wake model utilized for computing the extracted actual power from turbines and getting a wind velocity decay is the Jensens wake effect model, which is assumed to be the most used analytical model. In this model, the momentum is conserved inside the wake. After the wind flows through the turbine, the wind speed decreases and the turbulence intensity increases, forming the wake. As depicted in Fig. 4(b)., the wake region can be modelled as a conical region.

The wind speed inside the wake region subject to only one wake is expressed as [4]:

$$u = u_\infty \left[1 - \frac{2a}{\left(1 + \alpha \frac{x}{r_1}\right)^2} \right] \quad (10)$$

where, $a = \frac{1 - \sqrt{1 - C_T}}{2}$, $\alpha = \frac{0.5}{\ln(h/z_0)}$, $r_1 = r\sqrt{\frac{1-a}{1-2a}}$ u_∞ is the free incident wind speed, a is the axial induction factor, α the entrainment constant, x is the distance between upstream and downstream turbine, C_T is the wind turbine thrust coefficient, r_1 is the downstream rotor radius, r is the
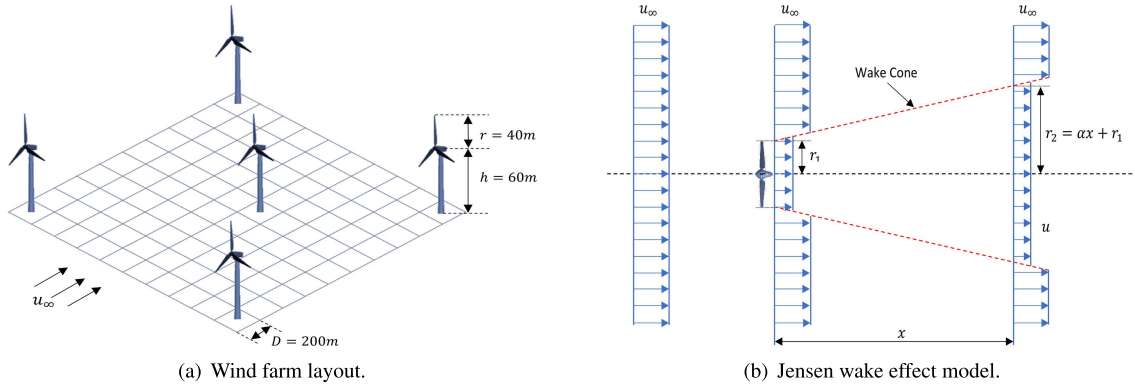
(a) Wind farm layout.

(b) Jensen wake effect model.

FIGURE 4. Schematic of wind farm layout and Jensen wake effect model.

rotor radius, h is the hub height of the turbines, z_0 is the surface roughness of wind farm.

The radius of the wake region r_2 is a function of downwind distance x [4]:

$$r_2 = \alpha x + r_1 \qquad (11)$$

When multiple wakes flow, the wind speed of N turbines N_T can be calculated as below [4]:

$$u_i = u_\infty \left[1 - \sqrt{\sum_{i=1}^{N_T} \left(1 - \frac{u}{u_\infty} \right)^2} \right] \qquad (12)$$

B. POWER GENERATION MODEL

The power generated by i^{th} in kW turbine is given by [38]:

$$P_i = 0.5 \rho \pi r^2 u_i^3 \frac{C_p}{1000}, \quad i = 1, 2, \ldots, N_T \qquad (13)$$

where ρ, r, u_i, and C_p are the air density ($1.225 \, kg/m^3$), rotor radius, the wind speed approaching the wind turbine i, and power coefficient, respectively.

The total power output in a wind park is equal to the sum of the product of each turbine power [38]:

$$P_{total} = \sum_{k=0}^{350} \sum_{i=1}^{N_T} f_k P_i(u_i) \qquad (14)$$

where N_T is the total turbines number, f_k is the wind probability distribution for a wind speed at a specific direction k and $\sum_{k=0}^{350} f_k = 1$.

The farm efficiency is described by the following formula [38]:

$$\eta = \frac{P_{total}}{P_{total,\max}} \qquad (15)$$

where $P_{total,\max}$ is the maximum output power generated without any wake.

C. COST MODEL

The cost of a wind farm utilized by Mosetti *et al.* [2] is the same as applied in this paper. This cost is modelled by a

TABLE 2. Simulation data.

Property	Value
area	2000 m^2
Hub height h	60 m
Rotor diameter $2r$	40 m
Rotor efficiency C_P	0.4
Trust coefficient C_T	0.8888
Surface roughness z_0	0.3 m
Air density ρ	1.2254 kg/m^3

simple function that is related only to the number of turbines placed in the wind park.

Its mathematical expression can be represented by [2]:

$$\text{Cost} = N_T \left(\frac{2}{3} + \frac{1}{3} \exp\left(-0.00174 \, N_T^2 \right) \right) \qquad (16)$$

The objective function to be optimized in this work is the minimization of the cost per unit power generated, it can be defined as follows [38]:

$$\text{Objective Function} = \frac{\text{Cost}}{P_{total}} \qquad (17)$$

This considered cost model depends only on the number of turbines installed. Their design variables have a dimension of 100. Each element vector adopts 100 discrete integer values of either 0 or 1 ($X_{i,j} \in \{0, 1\}$ where $i, j = 1, 2, \ldots, 100$). A value of "1" means the location has a turbine, while "0" indicates the location is empty. Hence, the output configuration has an unfixed number of wind turbines up to 100 WTs. During the CMRFO optimization process, any fraction value of design variables is rounded off to the nearest integer value.

In the following section, two experiences have been carried out to demonstrate that CMRFO performs better than the original approach.

IV. RESULTS AND DISCUSSION

For evaluating the performance of an optimization algorithm, various benchmark functions must be employed. To this end, the authors of this paper have utilized CEC-2017 functions [94] existed in literature. Besides, a complex real-world optimization problem named wind farm layout

TABLE 3. Parameters settings of the tested algorithms.

Algorithms	Parameters	Values
ABC [95]	Number of food sources	SN/2
	Number of limit trials	$0.6 \times$ SN $\times D$
AOA [96]	α	5
	μ	0.499
HHO [97]	β	1.5
	E_0 variable	$\in [-1, 1]$
SCA [98]	Number of elites a	2
BWOA [99]	pp = procreate rate	0.8
	Pm = mutation rate	0.4
	CR = cannibalism rate	0.5
DDOA [100]	Maximum temperature	2000
	Cooling rate α	0.995
LFD [101]	Threshold	2
	Comparative scalar value CSV	0.5
	β	1.5
	α_1	10
	α_2	0.00005
	α_3	0.005
	∂_1	0.9
	∂_2	0.1
SSA [102]	Leader position update probability	0.5
MRFO	Somersault factor S	2

optimization (WFLO). The wind turbine properties based on preview studies are shown in Table 2. The employed benchmark tests comprise unimodal, multimodal, hybrid, and composite functions. This diversity of benchmark classification can help prove the reliability and ability to explore, exploit, and converge towards the global optimum solution of the proposed algorithm. Furthermore, the outcomes of the proposed CMRFO and MRFO on CEC-2017 test functions for a number of population size and maximum iterations of 50 and 1000, respectively, are compared to 8 significant novel approaches, named ABC [95], AOA [96], HHO [97], SCA [98], BWOA [99], DDOA [100], LFD [101], and SSA [102]. Table 3 provides the parameter settings of all these algorithms. Statistical testings such as min, mean, standard deviation, and Wilcoxon signed-rank test have been carried out over 50 independent runs.

All simulations and analyses are implemented on a personal computer core i5 with 4GB-RAM Processor @1:8GHz under Microsoft Windows 10 operating system using MATLAB 2020a programming software.

A. EVALUATION OF CMRFO ON CEC-2017 TEST ANALYSIS
In this study, the performance of CMRFO has been assessed using different sets of well-known functions, including the CEC-2017, in which some of them have global optima and others have more than one local optima. The descriptions of these selected functions, including lower, upper boundaries and minimum values, are summarized in Table 4. Function F1 represents a unimodal function, F3 to F9 represent multimodal functions, F10 to F19 represent hybrid functions, whereas F20 to F30 represent composite functions. In this experiment, the mentioned benchmark tests (F1-F30) have been addressed with various variants of CMRFO. It is worth mentioning that the unimodal functions are more suitable for assessing the potential performances of algorithms'

exploitation, whereas the exploration capability can be generally checked using the multimodal functions. Dissimilar to the stated type of functions, the complex and challenging benchmark tests under the name of hybrid and composition examine the local optima avoidance. These functions are particularly appropriate for testing the algorithms' ability to solve real-world problems.

Based on the statistical mean in Table 8, it can be observed that MRFO occupied the last average rank over its variants. The optimal findings are shown in bold text and underlined. Furthermore, these outcomes obviously show that CMRFO with the singer (CMRFO5) and quadratic (CMRFO10) chaotic maps outperform the standard MRFO in most CEC-2017 functions. As it can be seen, CMRFO5 holds the first rank for F3, F4, F5, F7, F8, F13, F14, F18, F19, F20, F21, F22, F24, F26, and F27; besides, it secures the second rank for F11, F12, F16, F17, F25, F29, and F30, also the third position for F12, F28. Additionally, CMRFO5 performs better than MRFO for F1, F10, F15, F23, and F28. The quadratic map CMRFO10 reaches first place for F11, F16, F28, F29, and second for F9, F20, F21, and F22. Then, CMRF2, CMRF3, CMRF6, CMRF7, CMRF8, and CMRF9 present their best results only (F6, F23), F10, F25, F1, F12, F15, respectively. Moreover, to prove the significant differences between the CMRFO variants, the Wilcoxon rank-sum test [103] is employed; it is considered a non-parametric test that is used to determine whether two independent sets of obtained results are different statistically or not. In this context, a significance level of less than 5% signifies that the algorithms are different. According to the p-values in Table 8, the singer CMRFO5 shows the ability to outstrip the MRFO in most tests suites significantly.

Table 9 outlines the statistical results corresponding to their min, mean and std of fitness values of the winner CMRFO5 and the state-of-the-art algorithms mentioned above. The optimal outcomes are shown in bold text and underlined. Over the 29 considered functions, CMRFO5 performs better in 20 test suites; it attains the lowest mean fitness value for the various types of benchmark functions. Additionally, it can be seen that the novel developed algorithms LFD and AOA achieve the worst results in most cases.

In order to analyze the convergence performance of the algorithms, the convergence curve for 1000 iterations and 50 populations is used as a qualitative metric. The best fitness values of all competitive algorithms have been plotted according to the best run. It is obvious from Fig. 5. that CMRFO5 has a steady and speed convergence acceleration toward the global optimum. Despite the fact that CMRFO5 fails to reach the optimum results for some functions, it holds second place afterwards: ABC for F6, F9, F11, F30, BWOA for F7, F8, HHO for F25, and SSA for F27, with a very small difference. Furthermore, to assert the converging capability and stability of the winner chaotic map CMRFO5 compared to the competitors mentioned above, intensive statistical analyses have been investigated regarding the empirical

TABLE 4. Descriptions of the benchmark functions CEC-2017.

No	Name	Dim	Range	fmin
Unimodal functions				
F1	Shifted and Rotated Bent Cigar Function	10	[-100,100]	100
Multimodal functions				
F3	Shifted and Rotated Rosenbrock's Function	10	[-100,100]	300
F4	Shifted and Rotated Rastrigin's Function	10	[-100,100]	400
F5	Shifted and Rotated Expanded Scaffer's F6 Function	10	[-100,100]	500
F6	Shifted and Rotated Lunacek BiRastriginFunction	10	[-100,100]	600
F7	Shifted and Rotated Non-Continuous Rastrigin's Function	10	[-100,100]	700
F8	Shifted and Rotated Levy Function	10	[-100,100]	800
F9	Shifted and Rotated Schwefel's Function	10	[-100,100]	900
Hybrid functions (N is basic number of functions)				
F10	Hybrid Function 1 (N = 3)	10	[-100,100]	1000
F11	Hybrid Function 2 (N = 3)	10	[-100,100]	1100
F12	Hybrid Function 3 (N = 3)	10	[-100,100]	1200
F13	Hybrid Function 4 (N = 4)	10	[-100,100]	1300
F14	Hybrid Function 5 (N = 4)	10	[-100,100]	1400
F15	Hybrid Function 6 (N = 4)	10	[-100,100]	1500
F16	Hybrid Function 6 (N = 5)	10	[-100,100]	1600
F17	Hybrid Function 6 (N = 5)	10	[-100,100]	1700
F18	Hybrid Function 6 (N = 5)	10	[-100,100]	1800
F19	Hybrid Function 6 (N = 6)	10	[-100,100]	1900
Composite functions (N is basic number of functions)				
F20	Composite Function 1 (N = 3)	10	[-100,100]	2000
F21	Composite Function 2 (N = 3)	10	[-100,100]	2100
F22	Composite Function 3 (N = 4)	10	[-100,100]	2200
F23	Composite Function 4 (N = 4)	10	[-100,100]	2300
F24	Composite Function 5 (N = 5)	10	[-100,100]	2400
F25	Composite Function 6 (N = 5)	10	[-100,100]	2500
F26	Composite Function 7 (N = 6)	10	[-100,100	2600
F27	Composite Function 8 (N = 6)	10	[-100,100]	2700
F28	Composite Function 9 (N = 6)	10	[-100,100]	2800
F29	Composite Function 10 (N = 3)	10	[-100,100]	2900
F30	Composite Function 11 (N = 3)	10	[-100,100]	3000

distribution of the results. The box plots of all approaches executed fifty times are depicted in Fig. 6. It is obvious from the smallest interquartile ranges and medians that the proposed CMRFO5 optimizer has consistent stability in most CEC2017 benchmark functions.

According to the Wilcoxon test, Table 5 reveals the p-values of all comparative algorithms along with the higher T+ and T− values. It is apparent that most of the obtained p-values are less than the assumed significant level 5% compared to other approaches. This signifies that CMRFO5 significantly improves the performance of the basic MRFO. In summary, the reported results affirm the remarkable influence of singer map CMRFO5 on the primary MRFO and reveal its good exploration and exploitation capability in dealing with various types of functions. Therefore, CMRFO5 is the recommended variant for dealing with the real-world problem of wind farm layout optimization WFLO, which will be discussed in the next section.

B. EVALUATION OF CMRFO5 ON WFLO PROBLEM

The wind farm layout problem has been handled in this work with the purpose of validating the performance of the proposed chaotic approach CMRFO with singer map. As previously mentioned, this selected wind farm has a square shape split into 100 grids which aims to install the optimal number of wind turbines out of 100 turbines in optimal positioning, and the spacing distance between turbines is

at least 100 m. In this present study, the two scenarios suggested by Mosetti and some latest studies have been investigated, in which the first considers a variable wind direction and steady wind speed, while the second case assumes a variable wind direction and a variable wind speed. The fitness function to be optimized is the minimization of the cost per unit of power production, along with the total power (KW) and efficiency. The simulation results are implemented with a population size of 30 and a maximum number of 300 iterations over 30 independent runs for each case study. The computational results are compared to the previous studies, including Mosetti, Grady and some newest researches. It is worth noting that in most preceding works, Mosetti and Grady are reputed for evaluating the performance of the improved meta-heuristic algorithms. Additionally, the outcomes of all rival approaches have been re-validated according to their optimal placement plotted in their papers.

1) SCENARIO 1: CONSTANT WIND SPEED, VARIABLE DIRECTION

In this case study, a single wind speed of 12 m/s blowing from 36 rotational wind directions are considered; it varied from 0° to 360° with 10° difference between two adjacent directions and a uniform probability of occurrence. Computational experiments of MRFO, its winner CMRFO5 and the mentioned competitor methods, as well as the AOA, SCA, SSA algorithms, are summarized in Table 6. The

IEEE *Access*

FIGURE 5. Comparison of convergence curves of CMRFO5 vs the state-of-the-art algorithms for CEC-2017 benchmark tests.

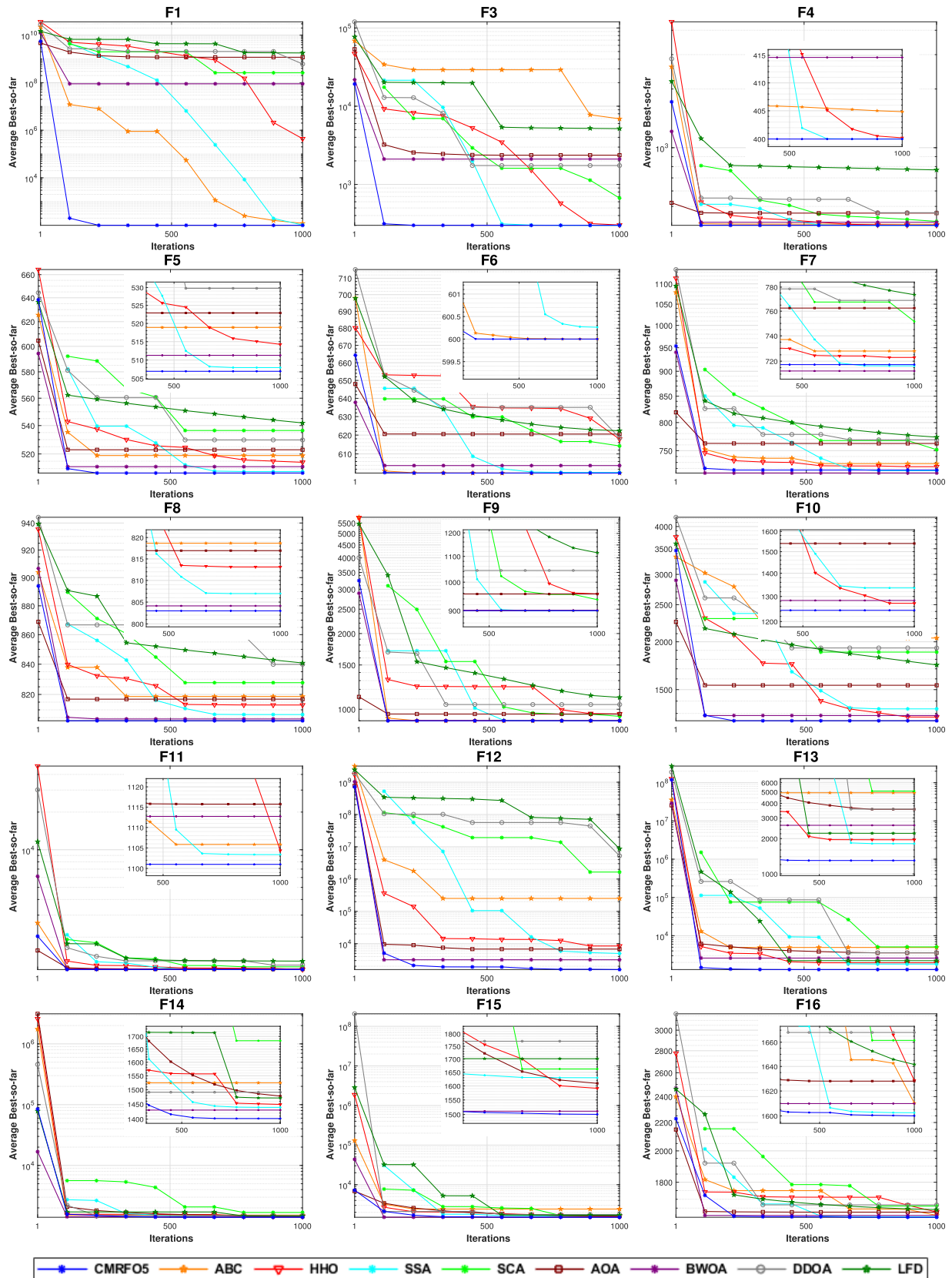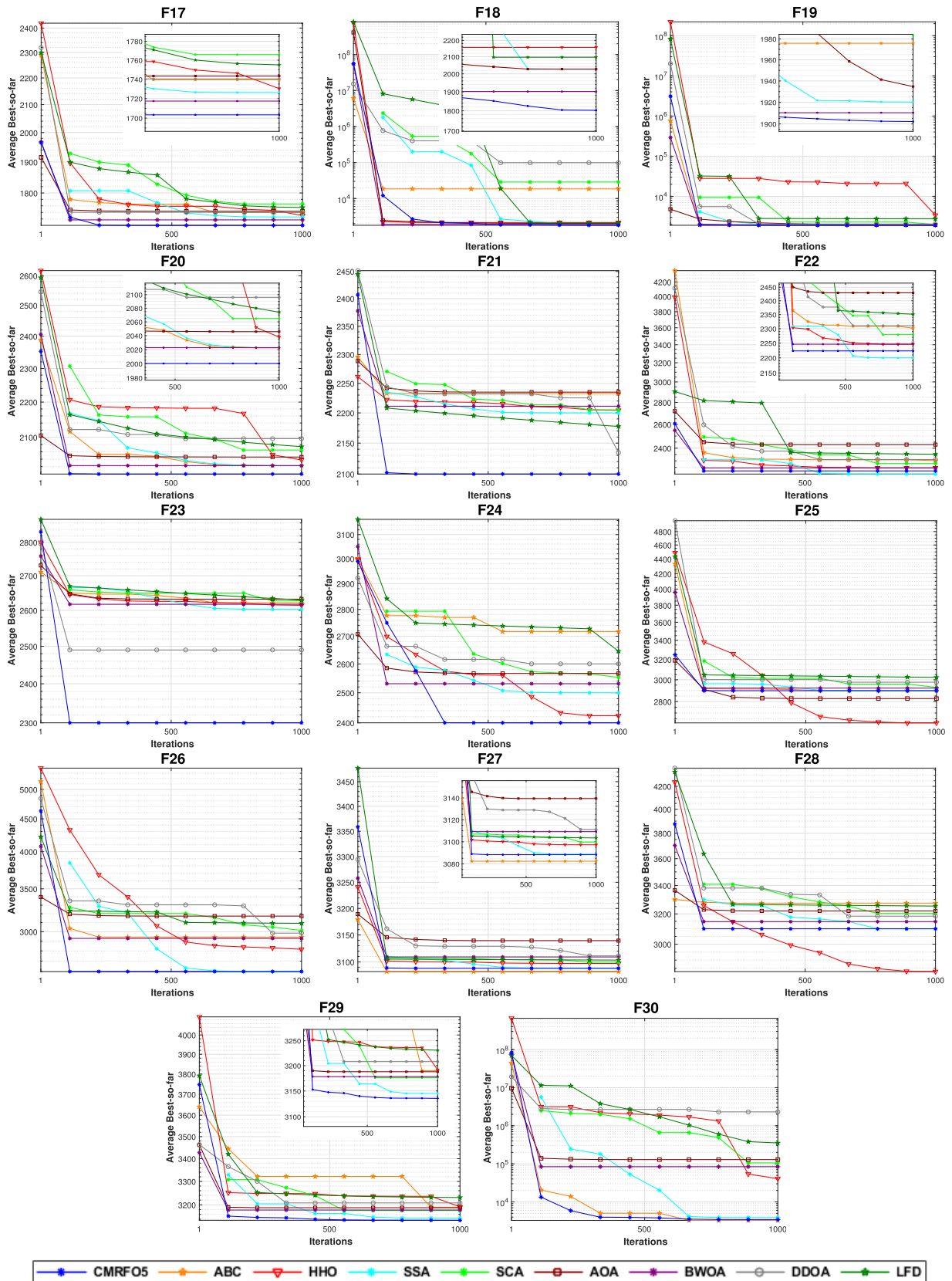**FIGURE 5.** *(Continued.)* Comparison of convergence curves of CMRFO5 vs the state-of-the-art algorithms for CEC-2017 benchmark tests.
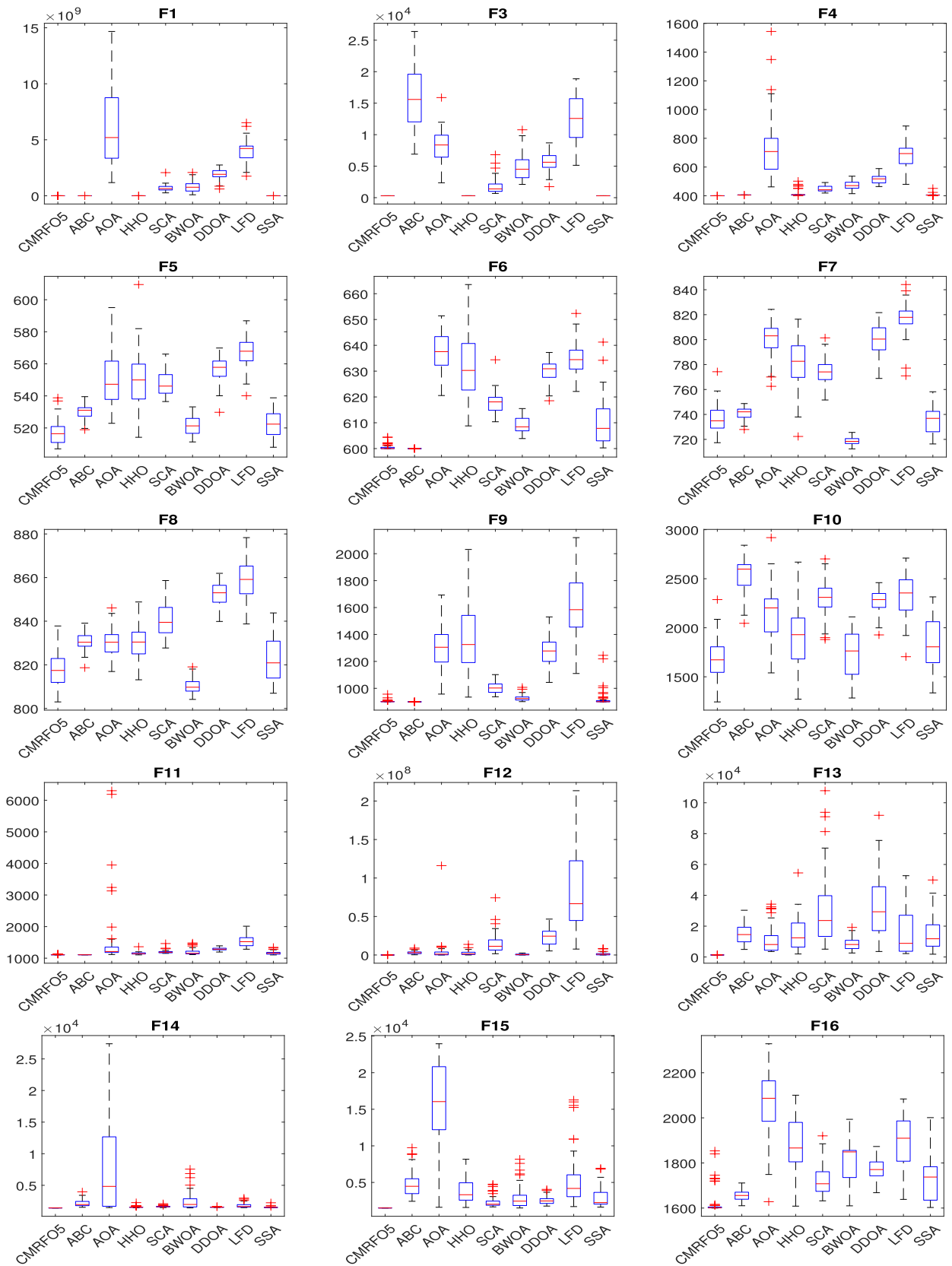
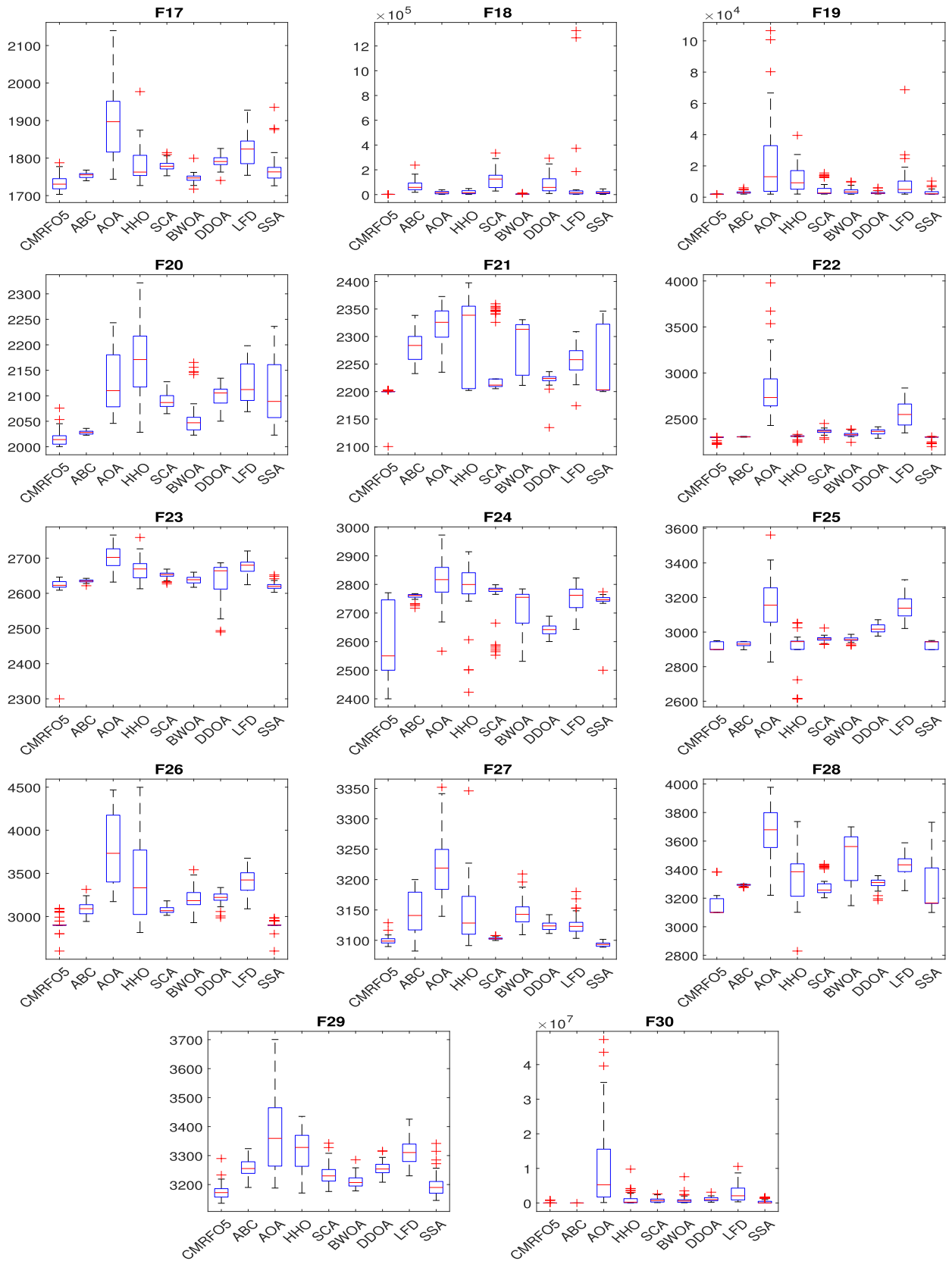**FIGURE 6.** Box plots of CMRFO and the state-of-the-art algorithm for CEC2017 problems.

FIGURE 6. *(Continued.)* Box plots of CMRFO and the state-of-the-art algorithm for CEC2017 problems.

TABLE 5. Statistical comparisons of CMRFO5 vs recent state-of-the-art algorithms for CEC-2017 benchmark tests.

No	ABC			AOA			HHO			SCA		
	p-value	T+	T-	p-value	T+	T-	p-value	T+	T-	p-value	T+	T-
F1	7.066×10^{-18}	1275	0	7.066×10^{-18}	1275	0	7.066×10^{-18}	1275	0	7.066×10^{-18}	1275	0
F3	3.311×10^{-20}	1275	0	3.311×10^{-20}	1275	0	3.311×10^{-20}	1275	0	3.311×10^{-20}	1275	0
F4	4.733×10^{-20}	1275	0	4.733×10^{-20}	1275	0	4.733×10^{-20}	1275	0	4.733×10^{-20}	1275	0
F5	2.777×10^{-13}	1246	29	1.193×10^{-16}	1275	0	9.848×10^{-16}	1254	21	1.005×10^{-17}	1275	0
F6	1.023×10^{-02}	255	1020	7.065×10^{-18}	1275	0	7.065×10^{-18}	1275	0	7.065×10^{-18}	1275	0
F7	6.536×10^{-03}	885	390	8.462×10^{-18}	1275	0	1.174×10^{-15}	1269	6	1.010×10^{-16}	1264	11
F8	1.401×10^{-12}	1249	26	1.835×10^{-11}	1219	56	1.611×10^{-10}	1179	96	1.065×10^{-16}	1273	2
F9	3.931×10^{-08}	66	1209	6.630×10^{-18}	1275	0	7.042×10^{-18}	1275	0	8.434×10^{-18}	1275	0
F10	1.013×10^{-17}	1274	1	1.338×10^{-12}	1246	29	9.409×10^{-05}	1037	238	1.605×10^{-16}	1273	2
F11	0.45026	681	594	1.064×10^{-17}	1275	0	2.682×10^{-15}	1268	7	6.993×10^{-18}	1275	0
F12	7.066×10^{-18}	1275	0	2.198×10^{-17}	1275	0	1.539×10^{-17}	1275	0	7.066×10^{-18}	1275	0
F13	7.066×10^{-18}	1275	0	7.066×10^{-18}	1275	0	7.066×10^{-18}	1275	0	7.066×10^{-18}	1275	0
F14	7.066×10^{-18}	1275	0	7.066×10^{-18}	1275	0	7.066×10^{-18}	1275	0	7.066×10^{-18}	1275	0
F15	7.066×10^{-18}	1275	0	7.066×10^{-18}	1275	0	7.066×10^{-18}	1275	0	7.066×10^{-18}	1275	0
F16	5.585×10^{-09}	977	298	1.366×10^{-17}	1275	0	8.379×10^{-16}	1257	18	2.444×10^{-11}	1218	57
F17	5.611×10^{-10}	1166	109	1.700×10^{-16}	1272	3	1.152×10^{-12}	1247	28	3.791×10^{-16}	1270	5
F18	7.066×10^{-18}	1275	0	7.066×10^{-18}	1275	0	7.066×10^{-18}	1275	0	7.066×10^{-18}	1275	0
F19	7.066×10^{-18}	1275	0	7.066×10^{-18}	1275	0	7.066×10^{-18}	1275	0	7.066×10^{-18}	1275	0
F20	8.762×10^{-09}	1108	167	1.729×10^{-17}	1275	0	2.192×10^{-17}	1275	0	1.283×10^{-17}	1275	0
F21	6.614×10^{-19}	1275	0	6.614×10^{-19}	1275	0	6.800×10^{-18}	1274	1	6.614×10^{-19}	1275	0
F22	4.444×10^{-15}	1259	16	7.066×10^{-18}	1275	0	1.471×10^{-14}	1146	129	1.174×10^{-15}	1271	4
F23	4.695×10^{-15}	1275	0	8.462×10^{-18}	1275	0	5.016×10^{-14}	1257	18	2.198×10^{-17}	1275	0
F24	2.032×10^{-11}	1212	63	2.524×10^{-12}	1242	33	1.464×10^{-13}	1232	43	1.188×10^{-13}	1139	136
F25	0.27297	876	399	6.491×10^{-15}	1263	12	4.1035×10^{-04}	826	449	7.411×10^{-12}	1267	8
F26	2.104×10^{-15}	1262	13	9.508×10^{-19}	1275	0	9.753×10^{-12}	1207	68	1.076×10^{-14}	1268	7
F27	7.801×10^{-12}	1233	42	7.063×10^{-18}	1275	0	4.156×10^{-12}	1224	51	1.721×10^{-05}	1019	256
F28	8.272×10^{-15}	1242	33	2.378×10^{-18}	1275	0	6.752×10^{-13}	1153	122	2.024×10^{-15}	1240	35
F29	3.791×10^{-16}	1271	4	1.202×10^{-16}	1273	2	1.110×10^{-15}	1270	5	2.142×10^{-14}	1234	41
F30	0.62208	465	810	4.206×10^{-17}	1275	0	8.942×10^{-14}	1149	126	1.551×10^{-14}	1203	72

No	BWOA			DDOA			LFD			SSA		
	p-value	T+	T-	p-value	T+	T-	p-value	T+	T-	p-value	T+	T-
F1	7.066×10^{-18}	1275	0	7.066×10^{-18}	1275	0	7.066×10^{-18}	1275	0	7.066×10^{-18}	1275	0
F3	3.311×10^{-20}	1275	0	3.311×10^{-20}	1275	0	3.311×10^{-20}	1275	0	1	1275	0
F4	4.733×10^{-20}	1275	0	4.733×10^{-20}	1275	0	4.733×10^{-20}	1275	0	4.733×10^{-20}	1275	0
F5	1.889×10^{-04}	1024	251	8.911×10^{-18}	1275	0	7.007×10^{-18}	1275	0	1.827×10^{-04}	984	291
F6	7.967×10^{-18}	1275	0	7.065×10^{-18}	1275	0	7.065×10^{-18}	1275	0	2.168×10^{-15}	1248	27
F7	7.075×10^{-16}	2	1273	7.969×10^{-18}	1275	0	7.504×10^{-18}	1275	0	0.62696	588	687
F8	2.392×10^{-08}	108	1167	7.025×10^{-18}	1275	0	7.025×10^{-18}	1275	0	1.887×10^{-02}	904	371
F9	4.777×10^{-14}	1212	63	6.630×10^{-18}	1275	0	6.630×10^{-18}	1275	0	0.34364	815	460
F10	0.18678	762	513	6.338×10^{-17}	1275	0	2.400×10^{-16}	1271	4	5.642×10^{-03}	938	337
F11	3.702×10^{-17}	1275	0	6.993×10^{-18}	1275	0	6.993×10^{-18}	1275	0	1.213×10^{-13}	1257	18
F12	1.907×10^{-16}	1273	2	7.066×10^{-18}	1275	0	7.066×10^{-18}	1275	0	2.954×10^{-17}	1275	0
F13	7.066×10^{-18}	1275	0	7.066×10^{-18}	1275	0	7.066×10^{-18}	1275	0	7.066×10^{-18}	1275	0
F14	2.071×10^{-17}	1275	0	7.066×10^{-18}	1275	0	7.066×10^{-18}	1275	0	7.066×10^{-18}	1275	0
F15	8.484×10^{-17}	1273	2	7.066×10^{-18}	1275	0	7.066×10^{-18}	1275	0	7.066×10^{-18}	1275	0
F16	8.561×10^{-15}	1225	50	3.283×10^{-14}	1267	8	2.266×10^{-16}	1275	0	1.598×10^{-11}	1165	110
F17	2.569×10^{-05}	1048	227	1.274×10^{-16}	1272	3	2.954×10^{-17}	1275	0	2.767×10^{-10}	1223	52
F18	7.504×10^{-18}	1275	0	7.066×10^{-18}	1275	0	7.066×10^{-18}	1275	0	7.066×10^{-18}	1275	0
F19	8.462×10^{-18}	1275	0	7.066×10^{-18}	1275	0	7.066×10^{-18}	1275	0	7.066×10^{-18}	1275	0
F20	5.864×10^{-14}	1247	28	1.073×10^{-17}	1275	0	8.961×10^{-18}	1275	0	7.984×10^{-17}	1272	3
F21	6.614×10^{-19}	1275	0	1.427×10^{-17}	1226	49	1.427×10^{-17}	1271	4	5.042×10^{-15}	1205	70
F22	1.010×10^{-16}	1237	38	1.174×10^{-15}	1271	4	7.066×10^{-18}	1275	0	1.358×10^{-04}	856	419
F23	1.851×10^{-13}	1253	22	3.477×10^{-05}	858	417	1.733×10^{-17}	1275	0	0.26556	714	561
F24	5.215×10^{-07}	1068	207	0.73657	886	389	1.864×10^{-07}	1182	93	3.019×10^{-05}	1087	188
F25	3.360×10^{-15}	1263	12	7.028×10^{-18}	1275	0	7.028×10^{-18}	1275	0	0.38492	757	518
F26	1.301×10^{-17}	1274	1	2.297×10^{-16}	1275	0	1.225×10^{-18}	1274	1	2.823×10^{-09}	920	355
F27	1.538×10^{-17}	1273	2	1.349×10^{-16}	1274	1	5.969×10^{-16}	1272	3	8.158×10^{-11}	38	1237
F28	4.275×10^{-16}	1250	25	3.104×10^{-14}	1229	46	8.738×10^{-18}	1275	0	3.398×10^{-08}	1082	193
F29	4.089×10^{-11}	1212	63	2.850×10^{-16}	1272	3	2.198×10^{-17}	1275	0	2.503×10^{-03}	1008	267
F30	9.926×10^{-14}	1202	73	5.643×10^{-16}	1267	8	7.551×10^{-17}	1265	10	3.100×10^{-12}	1155	120

CMRFO5 achieved a power generation of 18337 KW with 86.28% efficiency for a cost equal to **0.0015306**, while MRFO produced a total power of 17880 KW and 86.23% efficiency for a cost equal to 0.0015375. Along with these

TABLE 6. Simulation results of WFLO problem for case 1.

Authors		No. WT	Total Power (kW)	Efficiency (%)	Fitness Value
CMRFO5		41	18337	86.28	**0.0015306**
MRFO		40	17880	86.23	0.0015375
AOA		37	16530	86.18	0.0015611
SCA		36	16092	86.23	0.0015696
SSA		40	17692	85.32	0.0015539
Mosetti *et al.* [2]	Reported	19	9245	93.86	0.0017371
	Calculated	19	9234	93.75	0.0017378
Grady *et al.* [4]	Reported	39	17220	85.17	0.0015666
	Calculated	39	17204	85.09	0.0015649
Pookpunt *et al.* [14]	Reported	35	15796	87.06	0.0015648
	Calculated	35	15796	87.06	0.0015648
Taleb *et al.* [30]	Reported	40	15853	86.85	0.0015322
Kalyan *et al.* [31]	Reported	40	17781	85.74	0.0015461
	Calculated	40	17781	85.75	0.0015461
Partha *et al.* [38]	Reported	40	17920	86.42	0.0015341
	Calculated	40	17920	86.42	0.0015341
Hegazy *et al.* [43]	Reported	40	17878	86.22	0.0015380
	Calculated	40	17878	86.22	0.0015377
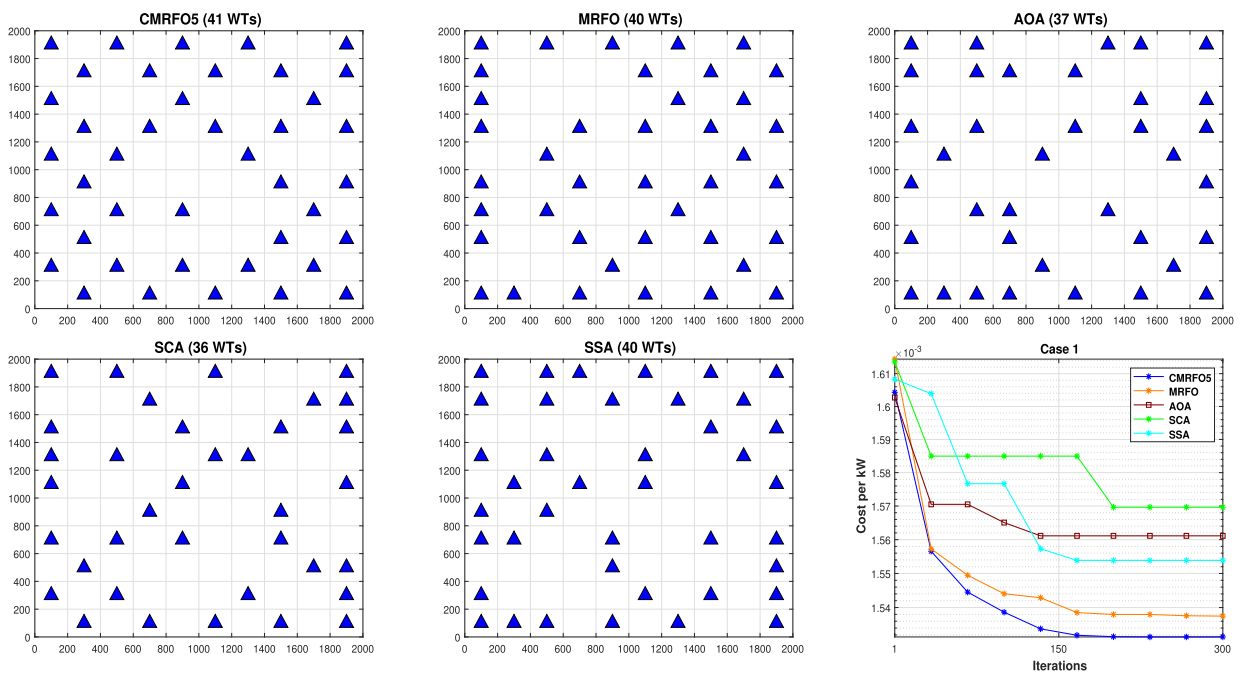
FIGURE 7. Optimal configurations and Convergence curves of CMRFO5 vs MRFO, AOA, SCA, SSA for Case 1.

findings, it is observed that the cost per unit power is improved compared to those reported in the literature and the re-implemented approaches and has been decreased by 11.92% for Mosetti *et al.* [2], 2.19% for Grady *et al.* [4], 2.18% for Pookpunt *et al.* [14], 0.10% for Taleb *et al.* [30], 1% for Kalyan *et al.* [31], 0.23% for Biswas *et al.* [38], 0.46% for Hegazy *et al.* [43], and 1.95%, 2.48%, 1.5% for AOA, SCA, and SSA, respectively. It is worth noting that the results are compared for unfixed WTs. Total wind turbines placed in this present case study are better than all approaches; it is reported that 41 number of turbines with a lower cost and a higher output total power. Moreover, regarding these earlier researches reported in Table 6, it can be seen that the Mosetti results found a better farm efficiency

of 93.75% and a worst total power output of 9234 KW for a minimum number of wind turbines equal to 19 machines. Furthermore, Pookpunt reaches the second rank in regard to efficiency, which is equal to 87.06%, and a smaller power output of 15796 KW for a number of wind turbines equal to 35. Besides, the optimal layouts corresponding to 39 and 40 machines have close results with each other, except that of Taleb *et al.* which gives a decreased cost with the lowest total power. Along these lines, it is obvious that the increased number of turbines affects an increase in power output and a reduction in efficiency. Fig. 7. describes the corresponding optimal configurations for CMRFO5, MRFO and the other competitive algorithms AOA, SCA, and SSA. Furthermore, the convergence curves of the fitness values for all approaches

TABLE 7. Simulation results of WFLO problem for case 2.

Authors		No. WT	Total Power (kW)	Efficiency (%)	Fitness Value
CMRFO5		40	33052	86.34	**0.0008317**
MRFO		40	32884	85.90	0.0008360
AOA		39	31805	85.22	0.0008465
SCA		35	28933	86.38	0.0008543
SSA		39	31900	85.47	0.0008439
Mosetti *et al.* [2]	Reported	15	13460	94.62	0.0009941
	Calculated	15	13588	94.65	0.0009847
Grady *et al.* [4]	Reported	39	32038	86.62	0.0008403
	Calculated	39	31827	85.27	0.0008458
Pookpunt *et al.* [14]	Reported	46	39359	89.83	0.0007894
	Calculated	46	36440	82.78	0.0008522
Taleb *et al.* [30]	Reported	39	32255	86.97	0.0008350
Kalyan *et al.* [31]	Reported	39	32498	86.11	0.0008377
	Calculated	39	32139	86.11	0.0008377
Partha *et al.* [38]	Reported	39	32351	86.68	0.0008322
	Calculated	39	32342	86.66	0.0008324
Hegazy *et al.* [43]	Reported	40	33005	87	0.0008330
	Calculated	40	32901	85.95	0.0008355
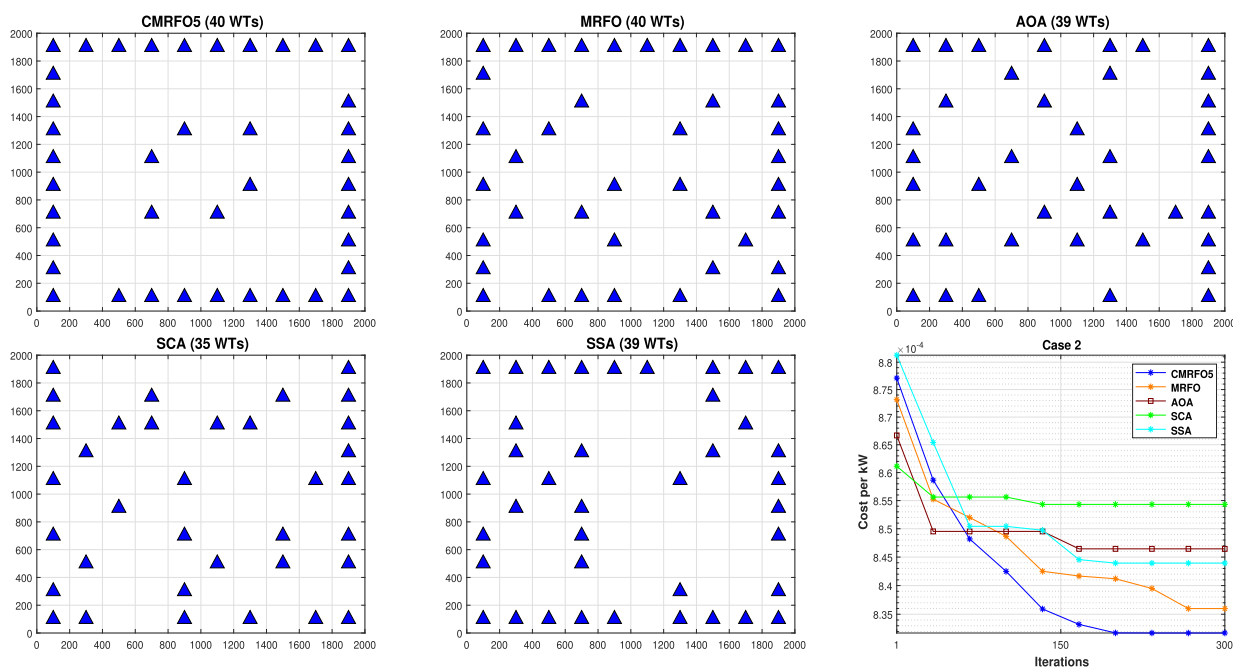
FIGURE 8. Optimal configurations and Convergence curves of CMRFO5 vs MRFO, AOA, SCA, SSA for Case 2.

are illustrated in Fig. 7. As can be seen, this figure reveals that CMRFO5 converges faster to lower fitness compared to the other approaches.

2) SCENARIO 2: VARIABLE WIND SPEED, VARIABLE DIRECTION

The variation of wind direction in this case study is identical to that of the previous scenario; however, the wind speed is assumed to be variable 8 m/s, 12 m/s, and 17 m/s, with a different occurrence probability. As tabulated in Table 7, CMRFO5 attains the best layout, which extracts a total power output of 33052 KW for 40 wind turbines with an efficiency of 86.34%, in addition to a best minimum cost value of **0.0008317**. Whereas the MRFO obtains a fitness value equal to 0.0008360 with a power output of 32884 KW and an efficiency of 85.90% for the same

wind turbines number as CMRFO5. Through the results found, it can be clearly seen that according to the fitness value, the proposed CMRFO5 algorithm yields better results than the other approaches; it is reduced by 15.54%, 1.67%, 2.41%, 0.40%, 0.72%, 0.08%, 0.45%, 1.75%, 2.65%, and 1.45%, compared with Mosetti *et al.* [2], Grady *et al.* [4], Pookpunt *et al.* [14], Taleb *et al.* [30], Kalyan *et al.* [31], Biswas *et al.* [38], Hegazy *et al.* [43], AOA, SCA, and SSA, respectively. According to the studies mentioned above, Mosetti reported higher efficiency of up to 94.65% with a lower total power output of 13588 KW for 15 turbines. While, Pookpunt demonstrated better power output of up to 36440 KW with the worst efficiency of 82.78% for a number of turbines equal to 46 machines, which confirms the relationship between the number of turbines in dealing with the farm efficiency and the output power. Through these

TABLE 8. Statistical results of MRFO and its variants on the 10 dimensional CEC-2017 benchmark tests.

No	Stats	MRFO	CMRFO1	CMRFO2	CMRFO3	CMRFO4	CMRFO5	CMRFO6	CMRFO7	CMRFO8	CMRFO9	CMRFO10
F1	Mean	2097.573	100.1421	100.1152	100.2464	100.0899	100.1184	100.2784	**100.0359**	100.0395	100.1761	100.1240
	Std	1981.0906	0.3458	0.4061	1.6103	0.2719	0.3689	1.2796	0.0876	0.1281	0.8891	0.3936
	p-value	N/A	0.18×10^{-16}	0.23×10^{-16}	0.12×10^{-16}	0.15×10^{-16}	0.18×10^{-16}	0.14×10^{-16}	0.15×10^{-16}	0.13×10^{-16}	0.18×10^{-16}	0.19×10^{-16}
F3	Mean	300	300	300	300	300	**300**	300	300	300	300	300
	Std	1.82×10^{-14}	4.06×10^{-14}	3.35×10^{-14}	3.81×10^{-14}	3.15×10^{-14}	3.15×10^{-14}	3.25×10^{-14}	3.54×10^{-14}	3.45×10^{-14}	3.54×10^{-14}	3.54×10^{-14}
	p-value	N/A	0.000133	0.004008	0.001056	0.013047	0.013047	0.007313	0.001126	0.002149	0.001126	0.006867
F4	Mean	400.131	400	400	400	400	**400**	400	400	400	400	400
	Std	0.1862	1.04×10^{-08}	1.87×10^{-09}	3.60×10^{-10}	2.41×10^{-10}	1.03×10^{-04}	5.34×10^{-08}	2.99×10^{-09}	5.65×10^{-11}	4.10×10^{-07}	2.62×10^{-09}
	p-value	N/A	0.68×10^{-17}	0.70×10^{-17}	0.70×10^{-17}	0.69×10^{-17}	0.71×10^{-17}	0.70×10^{-17}	0.70×10^{-17}	0.70×10^{-17}	0.70×10^{-17}	0.70×10^{-17}
F5	Mean	520.0583	521.2722	520.3767	519.5211	521.1727	**516.9541**	519.143	520.8762	520.5558	519.5609	519.9588
	Std	10.9221	7.6882	9.5459	8.399	10.8565	7.1322	9.3347	10.6724	9.4851	8.6519	9.1574
	p-value	N/A	0.196	0.674	0.8119	0.5417	0.2069	0.8039	0.669	0.5693	0.8685	0.8361
F6	Mean	600.3673	601.2773	**600.2466**	600.8839	601.0143	600.5113	600.4155	600.6223	601.0446	600.3579	600.6541
	Std	1.0691	2.3148	0.6791	1.767	1.985	1.0269	1.2742	1.4251	1.5694	0.7673	1.3301
	p-value	N/A	0.82×10^{-06}	0.00021	3.65×10^{-06}	2.95×10^{-07}	0.001725	0.000899	1.66×10^{-05}	5.66×10^{-07}	0.014896	5.57×10^{-05}
F7	Mean	738.2276	737.3985	738.3651	740.4357	740.74557	**737.1145**	741.5147	739.0989	743.560	739.0906	738.5482
	Std	13.6897	12.9944	14.3418	17.1498	12.5163	11.7301	14.0488	15.9511	16.9829	12.8629	14.4294
	p-value	N/A	0.87673	0.88217	0.69691	0.20587	0.88761	0.19615	0.86588	0.1152	0.60754	0.89852
F8	Mean	820.4364	820.6553	821.113	817.9888	818.4067	**817.8694**	819.4614	818.7052	821.1727	820.2175	818.9042
	Std	7.9093	7.2519	7.1105	8.7546	8.7162	7.8907	6.4329	7.9799	10.5546	7.5035	8.9173
	p-value	N/A	0.84691	0.5146	0.1001	0.10809	0.11756	0.59542	0.3224	0.83879	0.98349	0.2898
F9	Mean	**901.0928**	905.3002	903.8685	911.1309	904.2973	903.6283	905.7259	903.1203	908.7865	907.7559	902.6299
	Std	2.3416	15.3687	11.5525	31.9304	7.1251	9.021	12.6996	5.7436	16.6634	32.0578	6.7766
	p-value	N/A	2.30×10^{-05}	0.048169	4.09×10^{-05}	5.17×10^{-05}	0.001453	0.34×10^{-05}	0.001296	7.97×10^{-06}	0.021049	0.010004
F10	Mean	1733.079	1710.841	1650.347	**1633.621**	1703.807	1677.137	1683.402	1635.545	1788.829	1657.611	1636.241
	Std	255.8102	271.360	325.9786	268.6976	309.7243	230.7086	306.226	269.3882	264.5313	273.9412	268.5263
	p-value	N/A	0.93681	0.2237	0.085431	0.90397	0.47128	0.45864	0.098724	0.22889	0.28996	0.16065
F11	Mean	1110.235	1111.199	1109.968	1110.543	1112.459	1109.172	1112.708	1109.626	1111.648	1109.792	**1107.222**
	Std	7.2728	11.1417	7.2436	7.0104	10.0735	7.3677	11.5696	9.1464	9.1811	10.8018	5.09
	p-value	N/A	0.17×10^{-11}	0.45×10^{-10}	0.04×10^{-11}	0.21×10^{-10}	0.15×10^{-12}	0.23×10^{-12}	0.34×10^{-12}	0.71×10^{-11}	0.52×10^{-12}	0.95×10^{-11}
F12	Mean	14720.981	7523.205	5854.747	6853.126	8057.099	6139.737	8126.845	7057.930	**5211.294**	6542.096	7427.965
	Std	11100.60	8167.705	5441.902	7317.477	9413.227	7140.055	8259.906	9153.314	6559.616	6281.521	8702.721
	p-value	N/A	0.72255	0.42188	0.87129	0.38315	0.23708	0.62694	0.14864	0.96426	0.19853	0.007864
F13	Mean	1845.570	1341.012	1368.796	1348.710	1364.350	**1330.123**	1333.607	1337.466	1357.060	1338.732	1355.911
	Std	490.2762	46.8819	85.1153	72.0149	94.7453	37.7711	42.8626	48.9177	88.8647	62.319	102.7725
	p-value	N/A	0.43×10^{-04}	0.57×10^{-06}	0.62×10^{-05}	0.27×10^{-04}	0.38×10^{-06}	0.00017	0.13×10^{-05}	0.77×10^{-08}	0.45×10^{-05}	0.17×10^{-04}
F14	Mean	1441.234	1425.662	1422.853	1423.230	1426.426	**1419.358**	1425.065	1422.818	1419.424	1423.869	1422.640
	Std	10.5732	10.5593	13.0176	10.6737	14.5004	9.7909	11.8333	11.245	11.1055	9.5554	11.1913
	p-value	N/A	0.17×10^{-11}	0.17×10^{-09}	0.13×10^{-10}	0.57×10^{-07}	0.65×10^{-14}	0.83×10^{-09}	0.74×10^{-11}	0.13×10^{-12}	0.42×10^{-11}	0.31×10^{-11}
F15	Mean	1551.832	1512.795	1517.579	1514.496	1515.094	1513.823	1516.544	1517.122	1513.002	**1509.240**	1513.522
	Std	27.084	12.6681	18.5882	12.9492	13.3844	10.1424	17.0922	13.3365	15.097	8.8584	10.2843
	p-value	N/A	0.35×10^{-09}	0.74×10^{-11}	0.23×10^{-12}	0.85×10^{-12}	0.19×10^{-13}	0.48×10^{-11}	0.24×10^{-11}	0.13×10^{-12}	0.43×10^{-15}	0.25×10^{-13}
F16	Mean	1699.692	1654.407	1647.224	1678.250	1660.914	1627.396	1686.284	1659.668	1656.949	1651.765	**1624.964**
	Std	96.6835	88.3096	92.824	98.6938	80.2507	61.691	100.0328	82.4766	87.6941	83.2081	45.178
	p-value	N/A	0.023116	0.004557	0.26853	0.19615	0.000456	0.34318	0.034605	0.038951	0.016284	0.001152

TABLE 8. *(Continued.)* Statistical results of MRFO and its variants on the 10 dimensional CEC-2017 benchmark tests.

No	Stats	MRFO	CMRFO1	CMRFO2	CMRFO3	CMRFO4	CMRFO5	CMRFO6	CMRFO7	CMRFO8	CMRFO9	CMRFO10
F17	Mean	**1730.906**	1734.302	1742.851	1739.227	1738.697	1732.976	1740.438	1733.948	1738.724	1736.621	1737.918
	Std	19.4774	21.291	18.401	16.5471	19.0345	18.4703	22.5484	25.1026	24.0929	19.2864	19.4665
	p-value	N/A	0.56953	0.002083	0.016908	0.028115	0.5192	0.06618	0.79069	0.1168	0.16585	0.084185
F18	Mean	5266.412	1849.094	1837.650	1836.842	1841.319	**1831.475**	1833.161	1841.373	1831.954	1834.493	1839.684
	Std	3963.9691	36.7706	30.2554	29.4753	34.1606	25.0948	26.8113	36.1781	20.3735	23.4119	35.2247
	p-value	N/A	0.15×10^{-16}	0.11×10^{-16}	0.11×10^{-16}	0.11×10^{-16}	0.85×10^{-17}	0.95×10^{-17}	0.11×10^{-16}	0.90×10^{-17}	0.10×10^{-16}	0.14×10^{-16}
F19	Mean	1940.196	1907.731	1909.305	1907.71	1906.877	**1905.010**	1906.364	1906.844	1905.999	1905.160	1907.137
	Std	31.6386	6.2459	9.4789	6.2224	4.1106	3.0517	4.0026	8.0286	3.3636	2.9567	5.8103
	p-value	N/A	0.84×10^{-15}	0.27×10^{-13}	0.40×10^{-15}	0.67×10^{-16}	0.15×10^{-16}	0.47×10^{-16}	0.38×10^{-15}	0.21×10^{-16}	0.11×10^{-16}	0.19×10^{-15}
F20	Mean	2019.204	2021.986	2024.320	2024.502	2020.0145	**2016.492**	2027.570	2026.488	2029.472	2020.684	2016.744
	Std	13.4683	13.8541	22.8912	16.1367	13.6785	14.8198	24.5368	22.7432	18.3301	25.7883	14.6405
	p-value	N/A	0.20585	0.31916	0.15258	0.78804	0.13826	0.13287	0.10897	0.00552	0.5742	0.27145
F21	Mean	2207.781	2207.478	2205.218	2214.831	2202.416	**2198.510**	2209.484	2205.132	2215.707	2212.585	2200.306
	Std	27.3744	27.6319	22.6942	38.8256	15.6643	14.2533	30.1718	22.3107	40.8907	36.5628	0.85468
	p-value	N/A	0.2582	0.51178	0.64903	0.030079	0.029352	0.78975	0.31437	0.46846	0.3972	0.021595
F22	Mean	2299.285	2296.352	2296.616	2297.364	2298.049	**2294.377**	2299.509	2296.076	2295.238	2299.578	2299.117
	Std	13.4659	18.6974	17.8578	20.0764	16.0871	21.8493	13.4598	20.328	20.2876	12.3381	15.081
	p-value	N/A	0.84964	0.87673	0.23437	1.0000	0.83615	0.49058	0.73292	0.54179	0.61721	0.31584
F23	Mean	2623.215	2610.014	**2609.677**	2618.775	2614.244	2618.086	2621.978	2623.292	2625.405	2621.319	2615.526
	Std	10.0785	64.8183	64.6926	8.2051	47.0857	46.8682	9.108	10.8377	10.2469	8.0734	46.6508
	p-value	N/A	0.54637	0.49275	0.047482	0.07143	0.50149	0.69691	0.95876	0.19855	0.50589	0.50589
F24	Mean	2645.364	2639.611	2666.839	2652.940	2670.467	**2617.792**	2637.538	2650.205	2671.155	2636.646	2643.363
	Std	121.8942	125.2977	117.9319	121.3604	118.3891	130.3928	128.2829	124.2159	118.8997	127.336	123.5607
	p-value	N/A	0.72636	0.34784	0.71108	0.084471	0.66669	0.89925	0.65621	0.049547	0.94961	0.89682
F25	Mean	2926.363	2924.140	2920.666	2930.653	2931.797	2920.031	**2911.196**	2920.543	2923.921	2922.562	2930.158
	Std	22.902	23.6923	24.3344	22.1875	21.8469	23.3299	50.3703	53.5412	23.4852	27.4467	26.3107
	p-value	N/A	0.31747	0.39834	0.098688	0.030657	0.35376	0.095163	0.86586	0.95601	0.33608	0.38865
F26	Mean	2902.715	2924.174	2920.931	2910.464	2927.537	**2895.736**	2910.682	2935.590	2918.266	2937.241	2918.4607
	Std	81.0566	72.9282	88.3753	84.3696	76.5973	99.2268	73.1941	104.2287	73.6738	67.4352	62.8099
	p-value	N/A	0.052922	0.054394	0.14872	0.006538	0.015042	0.067798	0.016306	0.019778	0.000533	0.010896
F27	Mean	3102.843	3102.741	3100.948	3101.256	3102.914	**3099.96**	3101.553	3103.895	3106.047	3101.696	3101.180
	Std	14.0252	10.013	6.5435	6.6579	7.4465	6.5504	7.1793	15.0561	15.2969	8.0154	8.5464
	p-value	N/A	0.15258	0.51697	0.22369	0.03895	0.96701	0.3574	0.081736	0.019259	0.46915	0.49929
F28	Mean	3224.024	3172.664	3132.7821	3160.5751	3173.3103	3139.6296	3168.2362	3192.8285	3181.2652	3164.6667	**3119.3295**
	Std	141.2499	137.8906	109.9723	123.7692	126.1408	77.1226	120.2117	141.2381	145.3184	110.5937	108.5022
	p-value	N/A	0.39593	0.25049	0.32443	0.47323	0.03368	0.12593	0.84728	0.22104	0.49815	0.12112
F29	Mean	3188.567	3186.335	3183.497	3181.938	3185.724	3175.528	3192.128	3196.197	3185.016	3180.431	**3170.467**
	Std	27.2441	34.2804	25.7617	26.2456	25.9548	27.313	38.5012	34.2694	33.1409	28.0777	23.0438
	p-value	N/A	0.45033	0.32253	0.22899	0.64169	0.009445	0.96426	0.41398	0.28372	0.12506	0.001181
F30	Mean	$1.10\times10^{+05}$	$1.52\times10^{+05}$	$0.86\times10^{+05}$	$1.68\times10^{+05}$	$1.03\times10^{+05}$	$0.86\times10^{+05}$	$1.52\times10^{+05}$	$1.69\times10^{+05}$	$1.19\times10^{+05}$	$1.03\times10^{+05}$	$2.01\times10^{+05}$
	Std	$2.79\times10^{+05}$	$3.18\times10^{+05}$	$2.48\times10^{+05}$	$3.32\times10^{+05}$	$2.69\times10^{+05}$	$2.49\times10^{+05}$	$3.19\times10^{+05}$	$3.32\times10^{+05}$	$2.87\times10^{+05}$	$2.71\times10^{+05}$	$3.53\times10^{+05}$
	p-value	N/A	0.27×10^{-04}	0.55×10^{-07}	0.38×10^{-04}	0.40×10^{-06}	0.20×10^{-07}	0.32×10^{-04}	0.000948	0.73×10^{-05}	0.74×10^{-07}	0.000838
Rank		11	7	3	6	10	1	8	5	9	4	2

TABLE 9. Statistical results of MRFO, CMRFO5, and recent state-of-the-art algorithms for CEC-2017 benchmark tests.

No	Stats	CMRFO5	MRFO	ABC	AOA	HHO	SCA	BWOA	DDOA	LFD	SSA
F1	Min	100	100.0178	104.1253	$11765 \times 10^{+05}$	18073.0793	$26103 \times 10^{+04}$	$89888 \times 10^{+03}$	$61104 \times 10^{+04}$	$17520 \times 10^{+05}$	102.6611
	Mean	**100.1184**	2097.5726	1396.5559	$61080 \times 10^{+05}$	367089.812	$70076 \times 10^{+04}$	$82828 \times 10^{+04}$	$19242 \times 10^{+05}$	$40097 \times 10^{+05}$	2461.5861
	Std	0.36895	1981.0906	2434.7704	$32658 \times 10^{+05}$	272042.856	$29806 \times 10^{+04}$	$50294 \times 10^{+04}$	$46369 \times 10^{+04}$	$10203 \times 10^{+05}$	2664.6494
F3	Min	300	300	6907.0694	2364.5342	300.4506	669.4676	2109.2407	1743.6912	5139.2863	300
	Mean	**300**	300	15934.051	8033.3806	301.6873	1773.4468	4911.2324	5609.9035	12667.789	300
	Std	3.15×10^{-14}	1.82×10^{-14}	5151.3014	2623.9994	0.81282	1212.5124	2026.4448	1447.2838	3702.0663	9.15×10^{-10}
F4	Min	400	400.0016	404.6338	461.9055	400.0834	419.0679	414.6165	464.2657	479.6992	400.0035
	Mean	**400**	400.131	405.6868	748.3511	418.6887	448.9998	473.4022	517.2639	687.0031	405.8495
	Std	0.000103	0.18617	0.274	232.0912	26.5822	19.2625	27.338	30.1383	88.2683	7.2882
F5	Min	506.9647	505.9697	518.9	522.8948	514.1694	536.4773	511.2835	529.7721	540.0721	507.9597
	Mean	**516.9541**	520.0583	529.9409	550.4531	550.1288	547.4939	521.6379	556.3508	566.7704	522.8465
	Std	7.1322	10.9221	4.1004	19.3692	17.8895	7.0818	5.9429	7.9848	8.6734	8.0716
F6	Min	600	600	600.0001	620.5485	608.785	610.3868	603.8795	618.5312	622.1313	600.2623
	Mean	600.5113	600.3673	**600.0006**	637.9537	631.3302	617.9957	609.063	630.1757	634.5783	610.1005
	Std	1.0269	1.0691	0.000547	7.236	11.6899	3.9539	3.0375	4.3916	6.0805	8.9165
F7	Min	717.3423	718.8392	727.9238	762.5366	722.3464	751.5879	712.4135	768.8683	770.9526	716.333
	Mean	737.1145	738.2276	740.9227	800.6055	781.3049	773.6834	**718.6622**	799.4081	817.3019	735.5679
	Std	11.7301	13.6897	4.8365	14.1751	18.8604	10.6426	**2.9405**	13.1215	12.5765	11.4014
F8	Min	802.9849	805.9698	818.6597	816.9260	813.1308	827.7127	804.1334	839.8767	838.7315	806.9647
	Mean	817.8694	820.4364	830.3386	830.3633	830.6293	840.3830	**810.0329**	852.482	859.2124	822.9039
	Std	7.8907	7.9093	3.8789	6.6514	8.1434	7.3276	**3.2466**	5.7841	8.9286	10.2899
F9	Min	900	900	900	957.1875	934.8182	937.3978	901.2887	1044.2472	1110.1635	900
	Mean	903.6283	901.0928	**900**	1318.7258	1381.61	1004.2918	928.0941	1281.4594	1590.1124	923.9426
	Std	9.021	2.3416	9.092×10^{-07}	174.0482	250.1831	38.3651	22.4807	120.9949	236.3869	68.3522
F10	Min	1243.8315	1312.6962	2045.595	1539.8016	1271.8121	1879.8585	1283.6307	1927.0878	1704.7719	1335.9077
	Mean	**1677.1372**	1733.0787	2549.2267	2158.0853	1924.2944	2305.4892	1734.1427	2273.7947	2328.9231	1826.104
	Std	230.7086	255.8102	166.3546	267.8692	332.4876	191.2879	229.6797	111.208	213.6471	260.7996
F11	Min	1100.995	1101.991	1105.6035	1115.7255	1104.1502	1151.6464	1112.7086	1194.9936	1283.8498	1103.3742
	Mean	1109.1719	1110.235	**1108.3025**	1592.7285	1153.2778	1200.0524	1193.7832	1287.8524	1542.4541	1165.5813
	Std	7.3677	7.2728	1.3005	1106.6402	39.0712	51.2447	91.2865	42.0288	165.1428	53.9057
F12	Min	1418.1468	1576.4888	251642.80	6786.59	8458.29	1649005	3169.6114	5256718	7682788	4936.69
	Mean	**6139.7371**	14720.9811	$30960 \times 10^{+02}$	$47035 \times 10^{+02}$	2666190	$15755 \times 10^{+03}$	744264.29	$24251 \times 10^{+03}$	$83181 \times 10^{+03}$	1508777.39
	Std	7140.0549	11100.5981	1723274.83	$16367 \times 10^{+03}$	2874531	$13609 \times 10^{+03}$	742262.79	$10671 \times 10^{+03}$	$50840 \times 10^{+03}$	2047571.04
F13	Min	1302.0134	1301.0296	4917.9339	3556.8576	1954.7416	5087.5675	2597.3715	3568.2548	2217.8035	1810.9977
	Mean	**1330.1229**	1845.5697	15406.1273	11308.8108	14685.457	31778.3576	8369.9657	33685.0613	16349.1861	14705.1368
	Std	37.7711	490.2762	6277.1276	9127.5776	10528.8749	24008.6383	3702.0104	20812.1108	15460.7087	10682.0534
F14	Min	1401.9899	1418.559	1524.4842	1477.0636	1449.1699	1477.6439	1430.014	1491.2249	1470.6712	1438.9911
	Mean	**1419.3578**	1441.2343	2122.9352	8050.3722	1557.6467	1649.7892	2531.1212	1540.5977	1804.465	1525.7306
	Std	9.7909	10.5732	510.4962	8029.022	122.5014	120.8306	1433.5194	32.4504	376.0068	117.1178
F15	Min	1500.2088	1510.2402	2425.3774	1609.3136	1582.1958	1662.5941	1511.0962	1770.2125	1701.4647	1629.7445
	Mean	**1513.8233**	1551.8319	4813.6167	15663.6831	3751.6238	2362.5041	2889.1888	2542.3852	5413.9798	2853.8631
	Std	10.1424	27.084	1755.1316	5257.2265	1609.0629	804.7872	1617.6799	516.1021	3791.37	1272.1191
F16	Min	1600.0219	1600.349	1610.2732	1628.0261	1608.5178	1632.0765	1609.862	1668.1162	1638.5112	1602.5192
	Mean	**1627.3958**	1699.6915	1656.9162	2069.255	1878.5048	1724.4419	1801.9117	1772.1934	1897.0009	1728.5368
	Std	61.691	96.6835	22.5655	143.8633	121.4399	65.0614	93.8844	45.8059	117.6753	109.4442
F17	Min	1703.3477	1701.718	1739.5189	1743.4245	1726.8772	1752.9925	1717.4384	1740.4005	1754.1786	1726.2664

TABLE 9. *(Continued.)* Statistical results of MRFO, CMRFO5, and recent state-of-the-art algorithms for CEC-2017 benchmark tests.

No	Stats	CMRFO5	MRFO	ABC	AOA	HHO	SCA	BWOA	DDOA	LFD	SSA
	Mean	1732.9763	**1730.9062**	1753.3206	1894.8271	1781.7098	1778.8731	1746.2963	1791.0506	1819.8408	1770.3044
	Std	18.4703	19.4774	7.0195	96.2881	45.6446	13.2039	12.3443	15.4929	39.1812	38.1312
F18	Min	1802.3609	1864.5561	18477.475	2027.2261	2156.2826	28646.288	1901.5941	8669.365	2096.7769	2026.6548
	Mean	**1831.4745**	5266.4123	68631.177	16227.555	18558.102	121514.735	4306.4942	85544.995	77239.175	17447.0587
	Std	25.0948	3963.9691	43243.905	9979.5705	13464.689	69175.198	2135.4314	71160.931	257452.658	11439.666
F19	Min	1900.6711	1908.2395	1975.8087	1934.7269	1979.3116	1983.2817	1910.3291	2047.196	1947.1354	1920.2902
	Mean	**1905.0104**	1940.1962	3140.6203	23225.399	11404.764	5092.9924	4031.3567	2799.5349	8423.1065	2942.4398
	Std	3.0517	31.6386	859.694	24824.1411	7902.8866	4485.9498	1932.124	868.9286	10542.068	1631.0557
F20	Min	2000.312	2000.312	2022.6279	2045.8318	2028.4065	2064.8318	2022.7563	2050.1699	2068.843	2022.7651
	Mean	**2016.4915**	2019.2039	2027.6732	2133.4025	2170.7308	2090.3139	2055.2607	2099.5555	2123.9272	2107.6999
	Std	14.8198	13.4683	3.3562	61.5859	77.2246	15.5265	35.2617	19.8881	37.0621	61.7107
F21	Min	2100	2200	2232.6869	2235.0465	2202.0304	2205.2296	2211.278	2134.5095	2174.2486	2200
	Mean	**2198.5103**	2207.7807	2282.81	2318.0154	2306.9123	2243.5206	2281.09	2222.0102	2256.8003	2255.537
	Std	14.2533	27.3744	28.0774	35.0129	69.7107	58.7958	46.5784	14.0774	24.3393	61.5842
F22	Min	2223.4439	2230.8422	2301.9761	2429.3177	2246.1528	2279.0935	2246.1956	2290.6514	2349.2804	2200
	Mean	**2294.3766**	2299.2845	2306.0737	2820.1521	2311.2681	2364.4225	2333.114	2359.9358	2562.2961	2295.4293
	Std	21.8493	13.4659	2.0097	305.4068	14.5599	26.1537	24.3549	28.3016	131.8384	24.4415
F23	Min	2300	2609.778	2621.6152	2631.9881	2612.9991	2627.0676	2617.1965	2490.0623	2624.5076	2602.8877
	Mean	**2618.0858**	2623.2152	2635.0097	2702.3875	2667.416	2652.696	2638.2439	2637.6187	2676.1679	2621.3689
	Std	46.8682	10.0785	4.0387	33.8882	30.2906	8.7391	10.3262	55.547	19.2904	10.0525
F24	Min	2400	2500	2717.1801	2566.6138	2423.1867	2552.8709	2531.0516	2600.2986	2642.6328	2500
	Mean	**2617.7919**	2645.3644	2758.0784	2809.2629	2788.9748	2755.5963	2717.9785	2642.9627	2753.7541	2743.1118
	Std	130.3928	121.8942	10.7342	73.0732	96.6027	70.5407	76.0115	20.4202	43.5004	36.0513
F25	Min	2897.7429	2897.7429	2897.9406	2826.1958	2614.0944	2928.8544	2921.5528	2976.815	3020.8231	2897.7457
	Mean	2920.0312	2926.3632	2929.8366	3158.9327	**2915.0283**	2959.4559	2958.1683	3020.1336	3140.3566	2926.6928
	Std	23.3299	22.902	13.5180	139.1985	89.2939	16.9835	13.2733	25.4794	67.765	23.2835
F26	Min	2600	2600	2943.1652	3173.0966	2814.4504	3013.9735	2928.8598	2984.7778	3089.6984	2600.0002
	Mean	**2895.7361**	2902.7154	3090.1683	3766.7459	3422.6353	3075.4684	3202.19	3214.4323	3411.6511	2903.3126
	Std	99.2268	81.0566	76.1166	388.4017	500.7396	40.1005	121.5204	72.353	139.8058	52.1753
F27	Min	3088.2834	3089.7479	3082.3692	3139.4707	3091.3629	3099.69	3109.1918	3111.2657	3103.2581	3088.7395
	Mean	3099.96	3102.8427	3147.1258	3222.7261	3142.4088	3102.8825	3145.6997	3123.6978	3125.7408	**3092.9233**
	Std	6.5504	14.0252	36.4590	48.2171	45.6239	1.6199	21.7126	6.9483	15.3302	3.0130
F28	Min	3100	3100	3274.5365	3220.5054	2829.9748	3202.8309	3147.7552	3184.5424	3252.7368	3100.0001
	Mean	**3139.6296**	3224.024	3292.6532	3664.8534	3327.1651	3291.0347	3491.9769	3302.0953	3431.6078	3235.3463
	Std	77.1226	141.2499	5.6190	171.1487	157.8645	74.7545	175.1864	37.7771	73.9556	134.2783
F29	Min	3135.5201	3143.8982	3190.0704	3187.9611	3170.8027	3176.1416	3178.1644	3208.0934	3230.1135	3145.2615
	Mean	**3175.5276**	3188.5672	3258.0053	3378.0624	3312.2524	3236.7101	3211.2884	3255.3683	3312.9168	3199.9829
	Std	27.313	27.2441	29.3141	130.0635	70.6285	33.7090	20.9899	26.1005	50.0444	43.6350
F30	Min	3547.927	3905.9333	3267.1926	129089.56	28305.04	105883.27	84071.09	231411.57	340339.913	3863.0929
	Mean	86424.038	109479.7439	**4265.3591**	11382700	1032816.9	899251.63	862177.61	1102934	2834144.16	370009.28
	Std	248811.34	279200.96	816.83	12987386	1737991	703039.82	1178717.51	576164.25	2307448.56	596442.87

analyses, CMRFO5 was able to find the optimal layout with a reasonable solution and a compromise between total power output and efficiency. The optimal locations of the current study for MRFO, CMRFO5 with singer map, and the state-of-the-art algorithms AOA, SCA, and SSA are plotted as depicted in Fig. 8. It can be evidently expected that the suggested chaotic approach attempts to install the wind turbines at the wind farm boundary. This is due to the low wind frequencies from straight all directions (0°, 90°, 180°, and 270°). This figure also shows the convergence curves of cost per unit throughout the simulation proceeding for basic MRFO; its variant CMRFO5, AOA, SCA, and SSA. To this end, the singer CMRFO5 converges faster than the original one and attains the minimum fitness value.

V. CONCLUSION

An optimal position of a wind turbine installed in a wind farm increases the overall power output and farm efficiency for a minimum cost. Accordingly, this study focuses on the development of a new inspired optimization approach, known as the manta ray foraging optimization MRFO algorithm, which is recommended in most academic studies. This algorithm was enhanced based on the chaotic sequences. To use this chaotic method, some MRFO's random values were replaced by chaotic maps that help in balancing between the intensification and diversification of algorithms and avoiding any entrapment in local optima. Ten chaotic maps have been embedded into the MRFO optimizer, supposedly ten improvement cases. To demonstrate the effectiveness of the proposed approaches, twenty-nine CEC-2017 benchmark functions were applied, and the best performing chaotic map out of ten chaotic sequences has been recommended to deal with the real word problem wind farm layout optimization WFLO, which includes two case studies. One with a constant wind speed and variable direction and one with both wind speed and direction are variables. Thus, the chaotic sequence that was found to be suitable for enhancing the MRFO is the singer map. Moreover, eight recent algorithms have been considered for comparison, including ABC, AOA, HHO, SCA, BWOA, DDOA, LFD, and SSA. Through the analysis of the results found for both experiments: CEC-2017 and WFLO problems, the CMRFO5 has the ability to balance between exploration and exploitation, and then to converge faster to the optimal solution, it is obviously that CMRFO-singer is often higher than the re-implemented well-known state-of-the-art algorithms, and those stated in the literature, in terms of optimization results and convergence speed. Further, the suggested approach provides an intriguing configuration of wind turbines that extracts a higher total output power and efficiency for the lowest cost. In accordance with these remarkable outcomes, The technique developed in this work is a useful approach for WF configuration. Thus, the authors recommend CMRFO with singer sequence to handle the WFLO for a realistic, higher dimensional problem that exceeds 100 variables as considered in this research and to deal with multiple types of WTs with a fixed number of WTs.

CONFLICT OF INTEREST

The authors declare that they have no conflict of interest.

APPENDIX A
COMPARISON RESULTS OF MRFO VS CMRFO5 AND RECENT STATE-OF-THE-ART ALGORITHMS FOR CEC-2017 BENCHMARK TESTS
See Tables 8 and 9.

REFERENCES

[1] RCCN. *The New Installed Capacity of Wind Power Will Break 60 GW in 2020*. Accessed: Jan. 13, 2021. [Online]. Available: http://en.rccn.com.cn/content_article_2839.html

[2] G. Mosetti, C. Poloni, and B. Diviacco, ''Optimization of wind turbine positioning in large windfarms by means of a genetic algorithm,'' *J. Wind Eng. Ind. Aerodyn.*, vol. 51, no. 1, pp. 105–116, Jan. 1994, doi: 10.1016/0167-6105(94)90080-9.

[3] N. O. Jensen, *A Note on Wind Generator Interaction*, vol. 2411. Roskilde, Denmark: Risø National Laboratory, Nov. 1983.

[4] S. A. Grady, M. Y. Hussaini, and M. M. Abdullah, ''Placement of wind turbines using genetic algorithms,'' *Renew. Energy*, vol. 30, no. 2, pp. 259–270, Feb. 2005, doi: 10.1016/j.renene.2004.05.007.

[5] A. M. Abdelsalam and M. A. El-Shorbagy, ''Optimization of wind turbines siting in a wind farm using genetic algorithm based local search,'' *Renew. Energy*, vol. 123, pp. 748–755, Aug. 2018, doi: 10.1016/j.renene.2018.02.083.

[6] N. Charhouni, M. Sallaou, and K. Mansouri, ''Realistic wind farm design layout optimization with different wind turbines types,'' *Int. J. Energy Environ. Eng.*, vol. 10, pp. 307–318, Apr. 2019, doi: 10.1007/s40095-019-0303-2.

[7] X. Ju and F. Liu, ''Wind farm layout optimization using self-informed genetic algorithm with information guided exploitation,'' *Appl. Energy*, vol. 248, pp. 429–445, Aug. 2019, doi: 10.1016/j.apenergy.2019.04.084.

[8] F. Liu, X. Ju, N. Wang, L. Wang, and W.-J. Lee, ''Wind farm macro-siting optimization with insightful bi-criteria identification and relocation mechanism in genetic algorithm,'' *Energy Convers. Manage.*, vol. 217, Aug. 2020, Art. no. 112964, doi: 10.1016/j.enconman.2020.112964.

[9] P.-Y. Yin, T.-H. Wu, and P.-Y. Hsu, ''Risk management of wind farm micro-siting using an enhanced genetic algorithm with simulation optimization,'' *Renew. Energy*, vol. 107, pp. 508–521, Jul. 2017, doi: 10.1016/j.renene.2017.02.036.

[10] Q. Yang, J. Hu, and S.-S. Law, ''Optimization of wind farm layout with modified genetic algorithm based on Boolean code,'' *J. Wind Eng. Ind. Aerodyn.*, vol. 181, pp. 61–68, Oct. 2018, doi: 10.1016/j.jweia.2018.07.019.

[11] H. Sun, H. Yang, and X. Gao, ''Investigation into spacing restriction and layout optimization of wind farm with multiple types of wind turbines,'' *Energy*, vol. 168, pp. 637–650, Feb. 2019, doi: 10.1016/j.energy.2018.11.073.

[12] S. Markarian, F. Fazelpour, and E. Markarian, ''Optimization of wind farm layout considering wake effect and multiple parameters,'' *Environ. Prog. Sustain. Energy*, vol. 38, no. 5, p. 13193, Mar. 2019, doi: 10.1002/ep.13193.

[13] C. Wan, J. Wang, G. Yang, H. Gu, and X. Zhang, ''Wind farm micro-siting by Gaussian particle swarm optimization with local search strategy,'' *Renew. Energy*, vol. 48, pp. 276–286, Dec. 2012, doi: 10.1016/j.renene.2012.04.052.

[14] S. Pookpunt and W. Ongsakul, ''Optimal placement of wind turbines within wind farm using binary particle swarm optimization with time-varying acceleration coefficients,'' *Renew. Energy*, vol. 55, pp. 266–276, Jul. 2013, doi: 10.1016/j.renene.2012.12.005.

[15] S. Pookpunt and W. Ongsakul, ''Design of optimal wind farm configuration using a binary particle swarm optimization at Huasai district, Southern Thailand,'' *Energy Convers. Manage.*, vol. 108, pp. 160–180, Jan. 2016, doi: 10.1016/j.enconman.2015.11.002.

[16] S. Chowdhury, J. Zhang, A. Messac, and L. Castillo, ''Unrestricted wind farm layout optimization (UWFLO): Investigating key factors influencing the maximum power generation,'' *Renew. Energy*, vol. 38, no. 1, pp. 16–30, Feb. 2012, doi: 10.1016/j.renene.2011.06.033.

[17] H. Long and Z. Zhang, "A two-echelon wind farm layout planning model," *IEEE Trans. Sustain. Energy*, vol. 6, no. 3, pp. 863–871, Jul. 2015, doi: 10.1109/TSTE.2015.2415037.

[18] M. Song, K. Chen, and J. Wang, "Three-dimensional wind turbine positioning using Gaussian particle swarm optimization with differential evolution," *J. Wind Eng. Ind. Aerodyn.*, vol. 172, pp. 317–324, Jan. 2018, doi: 10.1016/j.jweia.2017.10.032.

[19] P. P. Biswas, P. N. Suganthan, and G. A. J. Amaratunga, "Decomposition based multi-objective evolutionary algorithm for windfarm layout optimization," *Renew. Energy*, vol. 115, pp. 326–337, Jan. 2018, doi: 10.1016/j.renene.2017.08.041.

[20] L. Wang, J. Yuan, M. E. Cholette, Y. Fu, Y. Zhou, and A. C. Tan, "Comparative study of discretization method and Monte Carlo method for wind farm layout optimization under Weibull distribution," *J. Wind Eng. Ind. Aerodyn.*, vol. 180, pp. 1455–1481, Sep. 2018, doi: 10.1016/j.jweia.2018.07.021.

[21] K. Chen, M. X. Song, X. Zhang, and S. F. Wang, "Wind turbine layout optimization with multiple hub height wind turbines using greedy algorithm," *Renew. Energy*, vol. 96, pp. 676–686, Oct. 2016, doi: 10.1016/j.renene.2016.05.018.

[22] K. Yang, G. Kwak, K. Cho, and J. Huh, "Wind farm layout optimization for wake effect uniformity," *Energy*, vol. 183, pp. 983–995, Sep. 2019, doi: 10.1016/j.energy.2019.07.019.

[23] J. Park and K. H. Law, "Layout optimization for maximizing wind farm power production using sequential convex programming," *Appl. Energy*, vol. 151, pp. 320–334, Aug. 2015, doi: 10.1016/j.apenergy.2015.03.139.

[24] J. Feng and W. Z. Shen, "Solving the wind farm layout optimization problem using random search algorithm," *Renew. Energy*, vol. 78, pp. 182–192, Jun. 2015, doi: 10.1016/j.renene.2015.01.005.

[25] J. Feng and W. Z. Shen, "Wind farm power production in the changing wind: Robustness quantification and layout optimization," *Energy Convers. Manage.*, vol. 148, pp. 905–914, Sep. 2017, doi: 10.1016/j.enconman.2017.06.005.

[26] J. Feng and W. Z. Shen, "Design optimization of offshore wind farms with multiple types of wind turbines," *Appl. Energy*, vol. 205, pp. 1283–1297, Nov. 2017, doi: 10.1016/j.apenergy.2017.08.107.

[27] J. Feng, W. Shen, and Y. Li, "An optimization framework for wind farm design in complex terrain," *Appl. Sci.*, vol. 8, no. 11, p. 2053, Oct. 2018, doi: 10.3390/app8112053.

[28] J. Feng, W. Z. Shen, and C. Xu, "Multi-objective random search algorithm for simultaneously optimizing wind farm layout and number of turbines," *J. Phys., Conf. Ser.*, vol. 753, no. 3, Sep. 2016, Art. no. 032011, doi: 10.1088/1742-6596/753/3/032011.

[29] Y. Eroğlu and S. U. Seçkiner, "Design of wind farm layout using ant colony algorithm," *Renew. Energy*, vol. 44, pp. 53–62, Aug. 2012, doi: 10.1016/j.renene.2011.12.013.

[30] T. Nawal, B. Bachir, C. Saliha, H. Abdelkader, and R. El-Sehiemy, "Renewable energy sources scheduling approach for windfarm layout optimization by using ant lion optimization algorithm," *Appl. Mech. Mater.*, vol. 905, pp. 79–92, Feb. 2022, doi: 10.4028/p-1bvgm9.

[31] K. K. Kumar and G. N. Reddy, "The sparrow search algorithm for optimum position of wind turbine on a wind farm," *Int. J. Renw. Energy Res.*, vol. 11, no. 4, pp. 1939–1946, Dec. 2021, doi: 10.20508/ijrer.v11i4.12345.g8346.

[32] S. R. Reddy, "Wind farm layout optimization (WindFLO): An advanced framework for fast wind farm analysis and optimization," *Appl. Energy*, vol. 269, Jul. 2020, Art. no. 115090, doi: 10.1016/j.apenergy.2020.115090.

[33] M. Beskirli, I. Koc, and H. Kodaz, "Optimal placement of wind turbines using novel binary invasive weed optimization," *Tehnicki Vjesnik*, vol. 26, no. 1, pp. 56–63, Feb. 2019, doi: 10.17559/TV-20170725231351.

[34] I. Koc, "A comprehensive analysis of grid-based wind turbine layout using an efficient binary invasive weed optimization algorithm with levy flight," *Expert Syst. Appl.*, vol. 198, Jul. 2022, Art. no. 116835, doi: 10.1016/j.eswa.2022.116835.

[35] H. Hakli, "A new approach for wind turbine placement problem using modified differential evolution algorithm," *TURKISH J. Electr. Eng. Comput. Sci.*, vol. 27, no. 6, pp. 4659–4672, Nov. 2019, doi: 10.3906/elk-1901-192.

[36] M. Aslan, M. Gunduz, and M. S. Kiran, "A Jaya-based approach to wind turbine placement problem problem," *Energy Sources, A, Recovery, Utilization, Environ. Effects*, 2020, doi: 10.1080/15567036.2020.1805528.

[37] S. D. O. Turner, D. A. Romero, P. Y. Zhang, C. H. Amon, and T. C. Y. Chan, "A new mathematical programming approach to optimize wind farm layouts," *Renew. Energy*, vol. 63, pp. 674–680, Mar. 2014, doi: 10.1016/j.renene.2013.10.023.

[38] P. P. Biswas, P. N. Suganthan, and G. A. J. Amaratunga, "Optimal placement of wind turbines in a windfarm using L-SHADE algorithm," in *Proc. IEEE Congr. Evol. Comput. (CEC)*, Jun. 2017, pp. 83–88, doi: 10.1109/CEC.2017.7969299.

[39] S. Afanasyeva, J. Saari, O. Pyrhönen, and J. Partanen, "Cuckoo search for wind farm optimization with auxiliary infrastructure," *Wind Energy*, vol. 21, no. 10, pp. 855–875, May 2018, doi: 10.1002/we.2199.

[40] S. Rehman, S. S. Ali, and S. A. Khan, "Wind farm layout design using cuckoo search algorithms," *Appl. Artif. Intell.*, vol. 32, no. 11, pp. 899–922, Feb. 2017, doi: 10.1080/08839514.2017.1279043.

[41] J. C. Bansal and P. Farswan, "Wind farm layout using biogeography based optimization," *Renew. Energy*, vol. 107, pp. 386–402, Jul. 2017, doi: 10.1016/j.renene.2017.01.064.

[42] R. V. Rao and H. S. Keesari, "Multi-team perturbation guiding Jaya algorithm for optimization of wind farm layout," *Appl. Soft Comput.*, vol. 71, pp. 800–815, Oct. 2018, doi: 10.1016/j.asoc.2018.07.036.

[43] H. Rezk, A. Fathy, A. A. Z. Diab, and M. Al-Dhaifallah, "The application of water cycle optimization algorithm for optimal placement of wind turbines in wind farms," *Energies*, vol. 12, no. 22, p. 4335, Nov. 2019, doi: 10.3390/en12224335.

[44] S.-U.-R. Massan, A. I. Wagan, and M. M. Shaikh, "A new metaheuristic optimization algorithm inspired by human dynasties with an application to the wind turbine micrositing problem," *Appl. Soft Comput.*, vol. 90, May 2020, Art. no. 106176, doi: 10.1016/j.asoc.2020.106176.

[45] M. A. M. Ramli and H. R. E. H. Bouchekara, "Wind farm layout optimization considering obstacles using a binary most valuable player algorithm," *IEEE Access*, vol. 8, pp. 131553–131564, 2020, doi: 10.1109/ACCESS.2020.3009046.

[46] S. Shamshirband, D. Petkovic, R. Hashim, and S. Motamedi, "Adaptive neuro-fuzzy methodology for noise assessment of wind turbine," *PLoS ONE*, vol. 9, no. 7, Jul. 2014, Art. no. 103414, doi: 10.1371/journal.pone.0103414.

[47] B. L. D. Pont and J. Cagan, "An extended pattern search approach to wind farm layout optimization," *J. Mech. Des.*, vol. 134, no. 8, pp. 677–686, Aug. 2012, doi: 10.1115/1.4006997.

[48] W. Zhao, Z. Zhang, and L. Wang, "Manta ray foraging optimization: An effective bio-inspired optimizer for engineering applications," *Eng. Appl. Artif. Intell.*, vol. 87, Jan. 2020, Art. no. 103300, doi: 10.1016/j.engappai.2019.103300.

[49] A. Fathy, H. Rezk, and D. Yousri, "A robust global MPPT to mitigate partial shading of triple-junction solar cell-based system using Manta ray foraging optimization algorithm," *Sol. Energy*, vol. 207, pp. 305–316, Sep. 2020, doi: 10.1016/j.solener.2020.06.108.

[50] F. A. Alturki, H. O. Omotoso, A. A. Al-Shamma'a, H. M. H. Farh, and K. Alsharabi, "Novel Manta rays foraging optimization algorithm based optimal control for grid-connected PV energy system," *IEEE Access*, vol. 8, pp. 187276–187290, 2020, doi: 10.1109/ACCESS.2020.3030874.

[51] S. I. Selem, H. M. Hasanien, and A. A. El-Fergany, "Parameters extraction of PEMFC's model using manta rays foraging optimizer," *Int. J. Energy Res.*, vol. 44, no. 6, pp. 4629–4640, May 2020, doi: 10.1002/er.5244.

[52] M. A. El-Hameed, M. M. Elkholy, and A. A. El-Fergany, "Three-diode model for characterization of industrial solar generating units using Manta-rays foraging optimizer: Analysis and validations," *Energy Convers. Manage.*, vol. 219, Sep. 2020, Art. no. 113048, doi: 10.1016/j.enconman.2020.113048.

[53] S. Chattopadhyay, A. Dey, and H. Basak, "Optimizing speech emotion recognition using Manta-ray based feature selection," Sep. 2020, *arXiv:2009.08909*.

[54] M. A. Elaziz, D. Yousri, M. A. A. Al-Qaness, A. M. Abdelaty, A. G. Radwan, and A. A. Ewees, "A Grunwald–Letnikov based Manta ray foraging optimizer for global optimization and image segmentation," *Eng. Appl. Artif. Intell.*, vol. 98, Feb. 2021, Art. no. 104105, doi: 10.1016/j.engappai.2020.104105.

[55] M. Micev, M. Ćalasan, Z. M. Ali, H. M. Hasanien, and S. H. E. A. Aleem, "Optimal design of automatic voltage regulation controller using hybrid simulated annealing—Manta ray foraging optimization algorithm," *Ain Shams Eng. J.*, vol. 12, no. 1, pp. 641–657, Mar. 2021, doi: 10.1016/j.asej.2020.07.010.

[56] K. K. Ghosh, R. Guha, S. K. Bera, N. Kumar, and R. Sarkar, "S-shaped versus V-shaped transfer functions for binary Manta ray foraging optimization in feature selection problem," *Neural Comput. Appl.*, vol. 33, no. 17, pp. 11027–11041, Jan. 2021, doi: 10.1007/s00521-020-05560-9.

[57] P. Karrupusamy, "Hybrid Manta ray foraging optimization for novel brain tumor detection," *J. Trends Comput. Sci. Smart Technol.*, vol. 2, no. 3, pp. 175–185, Jul. 2020, doi: 10.36548/jscp.2020.3.005.

[58] M. A. Elaziz, K. M. Hosny, A. Salah, M. M. Darwish, S. Lu, and A. T. Sahlol, "New machine learning method for image-based diagnosis of COVID-19," *PLoS ONE*, vol. 15, no. 6, Jun. 2020, Art. no. 0235187, doi: 10.1371/journal.pone.0235187.

[59] M. G. Hemeida, S. Alkhalaf, A.-A.-A. Mohamed, A. A. Ibrahim, and T. Senjyu, "Distributed generators optimization based on multi-objective functions using Manta rays foraging optimization algorithm (MRFO)," *Energies*, vol. 13, no. 15, p. 3847, Jul. 2020, doi: 10.3390/en13153847.

[60] A. M. Shaheen, R. A. El-Sehiemy, A. M. Elsayed, and E. E. Elattar, "Multi-objective Manta ray foraging algorithm for efficient operation of hybrid AC/DC power grids with emission minimisation," *IET Gener., Transmiss. Distrib.*, vol. 15, no. 8, pp. 1314–1336, Dec. 2020, doi: 10.1049/gtd2.12104.

[61] F. Daqaq, S. Kamel, M. Ouassaid, R. Ellaia, and A. M. Agwa, "Non-dominated sorting Manta ray foraging optimization for multi-objective optimal power flow with wind/solar/small-hydro energy sources," *Fractal Fractional*, vol. 6, no. 4, p. 194, Mar. 2022, doi: 10.3390/fractalfract6040194.

[62] S. Arora and P. Anand, "Chaotic grasshopper optimization algorithm for global optimization," *Neural Comput. Appl.*, vol. 31, no. 8, pp. 4385–4405, Aug. 2019, doi: 10.1007/s00521-018-3343-2.

[63] S. Mugemanyi, Z. Qu, F. X. Rugema, Y. Dong, C. Bananeza, and L. Wang, "Optimal reactive power dispatch using chaotic bat algorithm," *IEEE Access*, vol. 8, pp. 65830–65867, 2020, doi: 10.1109/ACCESS.2020.2982988.

[64] E. V. Altay and B. Alatas, "Bird swarm algorithms with chaotic mapping," *Artif. Intell. Rev.*, vol. 53, no. 2, pp. 1373–1414, Feb. 2020, doi: 10.1007/s10462-019-09704-9.

[65] G. I. Sayed, A. E. Hassanien, and A. T. Azar, "Feature selection via a novel chaotic crow search algorithm," *Neural Comput. Appl.*, vol. 31, no. 1, pp. 171–188, Jan. 2019, doi: 10.1007/s00521-017-2988-6.

[66] G. Fuertes, M. Vargas, M. Alfaro, R. Soto-Garrido, J. Sabattin, and M. A. Peralta, "Chaotic genetic algorithm and the effects of entropy in performance optimization," *Chaos, Interdiscipl. J. Nonlinear Sci.*, vol. 29, no. 1, Jan. 2019, Art. no. 013132, doi: 10.1063/1.5048299.

[67] B. Alatas, "Uniform big bang–chaotic big crunch optimization," *Commun. Nonlinear Sci. Numer. Simul.*, vol. 16, no. 9, pp. 3696–3703, Sep. 2011, doi: 10.1016/j.cnsns.2010.12.025.

[68] G.-G. Wang, L. H. Guo, A. H. Gandomi, G.-S. Hao, and H. Q. Wang, "Chaotic krill herd algorithm," *Inf. Sci.*, vol. 274, pp. 17–34, Aug. 2014, doi: 10.1016/j.ins.2014.02.123.

[69] J. A. Rezaee, "A chaotic artificial immune system optimisation algorithm for solving global continuous optimisation problems," *Neural Comput. Appl.*, vol. 26, no. 4, pp. 827–833, May 2015, doi: 10.1007/s00521-014-1751-5.

[70] J. Too and A. R. Abdullah, "Chaotic atom search optimization for feature selection," *Arabian J. Sci. Eng.*, vol. 45, no. 8, pp. 6063–6079, Aug. 2020, doi: 10.1007/s13369-020-04486-7.

[71] G. I. Sayed, A. Tharwat, and A. E. Hassanien, "Chaotic dragonfly algorithm: An improved metaheuristic algorithm for feature selection," *Appl. Intell.*, vol. 49, no. 1, pp. 188–205, Jan. 2019, doi: 10.1007/s10489-018-1261-8.

[72] S. Mirjalili and A. H. Gandomi, "Chaotic gravitational constants for the gravitational search algorithm," *Appl. Soft Comput.*, vol. 53, pp. 407–419, Apr. 2017, doi: 10.1016/j.asoc.2017.01.008.

[73] B. Alatas, "Chaotic harmony search algorithms," *Appl. Math. Comput.*, vol. 216, no. 9, pp. 2687–2699, Jul. 2010, doi: 10.1016/j.amc.2010.03.114.

[74] S. Talatahari, B. F. Azar, R. Sheikholeslami, and A. H. Gandomi, "Imperialist competitive algorithm combined with chaos for global optimization," *Commun. Nonlinear Sci. Numer. Simul.*, vol. 17, no. 3, pp. 1312–1319, Mar. 2012, doi: 10.1016/j.cnsns.2011.08.021.

[75] M. Kohli and S. Arora, "Chaotic grey wolf optimization algorithm for constrained optimization problems," *J. Comput. Des. Eng.*, vol. 5, no. 4, pp. 458–472, Oct. 2018, doi: 10.1016/j.jcde.2017.02.005.

[76] Y. Sun, Y. Gao, and X. Shi, "Chaotic multi-objective particle swarm optimization algorithm incorporating clone immunity," *Mathematics*, vol. 7, no. 2, p. 146, Feb. 2019, doi: 10.3390/math7020146.

[77] Y. Xu, H. Chen, A. A. Heidari, J. Luo, Q. Zhang, X. Zhao, and C. Li, "An efficient chaotic mutative moth-flame-inspired optimizer for global optimization tasks," *Expert Syst. Appl.*, vol. 129, no. 1, pp. 135–155, Sep. 2019, doi: 10.1016/j.eswa.2019.03.043.

[78] G. I. Sayed, G. Khoriba, and M. H. Haggag, "A novel chaotic salp swarm algorithm for global optimization and feature selection," *Appl. Intell.*, vol. 48, no. 10, pp. 3462–3481, Oct. 2018, doi: 10.1007/s10489-018-1158-6.

[79] E. Yalçın, E. Çam, and M. C. Taplamacıoğlu, "A new chaos and global competitive ranking-based symbiotic organisms search algorithm for solving reactive power dispatch problem with discrete and continuous control variable," *Electr. Eng.*, vol. 102, no. 2, pp. 573–590, Jun. 2020, doi: 10.1007/s00202-019-00895-6.

[80] D. Yousri and S. Mirjalili, "Fractional-order cuckoo search algorithm for parameter identification of the fractional-order chaotic, chaotic with noise and hyper-chaotic financial systems," *Eng. Appl. Artif. Intell.*, vol. 92, Jun. 2020, Art. no. 103662, doi: 10.1016/j.engappai.2020.103662.

[81] H. Bouchekara, "Solution of the optimal power flow problem considering security constraints using an improved chaotic electromagnetic field optimization algorithm," *Neural Comput. Appl.*, vol. 32, no. 7, pp. 2683–2703, Apr. 2020, doi: 10.1007/s00521-019-04298-3.

[82] S. Saremi, S. Mirjalili, and A. Lewis, "Biogeography-based optimisation with chaos," *Neural Comput. Appl.*, vol. 25, no. 5, pp. 1077–1097, Oct. 2014, doi: 10.1007/s00521-014-1597-x.

[83] H. Dewar, P. Mous, M. Domeier, A. Muljadi, J. Pet, and J. Whitty, "Movements and site fidelity of the giant Manta ray, *Manta birostris*, in the Komodo Marine Park, Indonesia," *Mar. Biol.*, vol. 155, no. 2, pp. 121–133, Aug. 2008, doi: 10.1007/s00227-008-0988-x.

[84] Mantaray-World. *Manta Ray Facts*. Accessed: Dec. 26, 2020. [Online]. Available: https://www.mantaray-world.com/

[85] Manta Trust. *Mobulid Behavioural Ecology*. Accessed: Dec. 26, 2020. [Online]. Available: https://www.mantatrust.org/mobulid-behavioural-ecology

[86] E. N. Lorenz, "Deterministic non-periodic flow," *J. Atmos. Sci.*, vol. 20, no. 6, pp. 130–141, Mar. 1963, doi: 10.1175/1520-0469(1963)020<0130:DNF>2.0.CO;2.

[87] T.-Y. Li and J. A. Yorke, "Period three implies chaos," *Amer. Math. Monthly*, vol. 82, no. 10, pp. 985–992, Dec. 1975, doi: 10.1080/00029890.1975.11994008.

[88] Z. Zhang, H. Wang, and Y. Gao, "C2MP: Chebyshev chaotic map-based authentication protocol for RFID applications," *Pers. Ubiquitous Comput.*, vol. 19, no. 7, pp. 1053–1061, Oct. 2015, doi: 10.1007/s00779-015-0876-6.

[89] R. M. May, "Simple mathematical models with very complicated dynamics," *Nature*, vol. 261, pp. 459–467, Jun. 1976, doi: 10.1038/261459a0.

[90] N. Dong, X. Fang, and A.-G. Wu, "A novel chaotic particle swarm optimization algorithm for parking space guidance," *Math. Problems Eng.*, vol. 2016, pp. 1–14, Sep. 2016, doi: 10.1155/2016/5126808.

[91] M. Alizadeh, M. Alizadeh, and S. Ganjefar, "Simultaneous coordinated design of PSS and SSSC using improved Lozi map based chaotic optimization algorithm (ILCOA)," *Neurocomputing*, vol. 122, pp. 181–192, Dec. 2013, doi: 10.1016/j.neucom.2013.06.032.

[92] M. Joglekar, E. Ott, and J. A. Yorke, "Scaling of chaos versus periodicity: How certain is it that an attractor is chaotic?" *Phys. Rev. Lett.*, vol. 113, no. 8, Aug. 2014, Art. no. 084101, doi: 10.1103/PhysRevLett.113.084101.

[93] I. Katic, J. Højstrup, and N. O. Jensen, "A simple model for cluster efficiency," in *Proc. Eur. Wind Energy Assoc. Conf. Exhib. (EWEC)*, A. Raguzzi, Ed., Rome, Italy, 1986, pp. 407–410.

[94] N. H. Awad, M. Z. Ali, J. J. Liang, B. Y. Qu, and P. N. Suganthan, "Problem definitions and evaluation criteria for the Cec 2017 special session and competition on single objective bound constrained real-parameter numerical optimization," Nanyang Technol. Univ., Singapore, Tech. Rep., Nov. 2016.

[95] B. Basturk and D. Karaboga, "An artificial bee colony (ABC) algorithm for numeric function optimization," in *Proc. IEEE Swarm Intell. Symp.*, Indianapolis, IN, USA, May 2006, pp. 687–697.

[96] L. Abualigah, A. Diabat, S. Mirjalili, M. A. Elaziz, and A. H. Gandomi, "The arithmetic optimization algorithm," *Comput. Methods Appl. Mech. Eng.*, vol. 376, Apr. 2021, Art. no. 113609, doi: 10.1016/j.cma.2020.113609.

[97] A. A. Heidari, S. Mirjalili, H. Faris, I. Aljarah, M. Mafarja, and H. Chen, "Harris hawks optimization: Algorithm and applications," *Future Gener. Comput. Syst.*, vol. 97, pp. 849–872, Aug. 2019, doi: 10.1016/j.future.2019.02.028.

[98] S. Mirjalili, "SCA: A sine cosine algorithm for solving optimization problems," *Knowl.-Based Syst.*, vol. 96, pp. 120–133, Mar. 2016, doi: 10.1016/j.knosys.2015.12.022.

[99] V. Hayyolalam and A. A. P. Kazem, "Black widow optimization algorithm: A novel meta-heuristic approach for solving engineering optimization problems," *Eng. Appl. Artif. Intell.*, vol. 87, Jan. 2020, Art. no. 103249, doi: 10.1016/j.engappai.2019.103249.

[100] H. N. Ghafil and K. Jármai, "Dynamic differential annealed optimization: New metaheuristic optimization algorithm for engineering applications," *Appl. Soft Comput.*, vol. 93, Aug. 2020, Art. no. 106392, doi: 10.1016/j.asoc.2020.106392.

[101] E. H. Houssein, M. R. Saad, F. A. Hashim, H. Shaban, and M. Hassaballah, "Lévy flight distribution: A new metaheuristic algorithm for solving engineering optimization problems," *Eng. Appl. Artif. Intell.*, vol. 94, Sep. 2020, Art. no. 103731, doi: 10.1016/j.engappai.2020.103731.

[102] S. Mirjalili, A. H. Gandomi, S. Z. Mirjalili, S. Saremi, H. Faris, and S. M. Mirjalili, "Salp swarm algorithm: A bio-inspired optimizer for engineering design problems," *Adv. Eng. Softw.*, vol. 114, pp. 163–191, Dec. 2017, doi: 10.1016/j.advengsoft.2017.07.002.

[103] F. Wilcoxon, "Individual comparisons by ranking methods," *Biometrics Bull.*, vol. 1, no. 6, pp. 80–83, Dec. 1945, doi: 10.2307/3001968.

MOHAMMED OUASSAID (Senior Member, IEEE) received the Diploma of Agrégation degree in electrical engineering from the Ecole Nationale Supérieure d'Art et Métiers de Rabat (ex ENSET), Rabat, Morocco, in 1999, the M.Sc.A. and Ph.D. degrees in electrical engineering from the Mohammadia School of Engineers (EMI), Mohamed V University in Rabat, Rabat, in 2002 and 2006, respectively, and the Diploma degree from University's Habilitation, in 2012. From 2008 to 2015, he was a Professor at the National School of Applied Sciences of Safi (ENSA-Safi), Cadi Ayyad University, Marrakesh, Morocco. In 2015, he joined the Department of Electrical Engineering, Mohammadia School of Engineers, Mohammed V University in Rabat, where he is currently a Professor. He is the author or coauthor of numerous book chapters and articles in refereed journals and international conference proceedings. He is also involved in a number of research and teaching projects. His main research interests include electrical drives, power systems, control and optimization of renewable energy, integration of wind power and photovoltaic systems, and smart grid. He is a member of the IEEE Power and Energy Society.

FATIMA DAQAQ received the B.Tech. degree in mechanical engineering from Sultan Moulay Slimane University, Beni-Mellal, in 2012, and the M.Sc. degree in mechanics and engineering from Hassan II University of Casablanca, Casablanca, in 2014. She is currently pursuing the Ph.D. degree with the Mohammadia School of Engineers (EMI), Mohammed V University in Rabat. Her research interests include meta-heuristics, nature inspired computing, power system modeling, analysis, and simulation; and renewable energy systems, home energy management systems, and smart grid.

HOSSAM M. ZAWBAA was born in Cairo, Egypt, in 1987. He received the B.Sc. and M.Sc. degrees from the Faculty of Computers and Information, Cairo University, Giza, Egypt, in 2008 and 2012, respectively, and the Ph.D. degree from Babeş-Bolyai University, Cluj-Napoca, Romania, in 2018. He is currently an Assistant Professor at the Faculty of Computers and Artificial Intelligence, Beni-Suef University, Beni-Suef, Egypt. He has authored or coauthored over 80 research publications in peer-reviewed reputed journals and international conference proceedings. His research interests include computational intelligence, machine learning, computer vision, and natural language understanding. He has been rated as one of the top 2% scientists worldwide by Stanford in the field of AI, in 2020 and 2021. Moreover, he has been awarded the State Encouragement Award in the field of engineering sciences from the Academy of Scientific Research and Technology, Egypt, in 2020.

RACHID ELLAIA received the Ph.D. degree (3rd cycle) in applied mathematics and optimization from Paul Sabatier University, Toulouse, France, in 1984, and the Ph.D. degree in applied and computational mathematics from Mohammed V University in Rabat, Rabat, Morocco, in 1992. He has held a Visiting Professor positions at Toulouse University, Chile University, INSA of Rouen, Nice Sophia Antipolis University, Haute Alsace University, and INRIA Lille. He is currently a Full Professor at the Mohammadia School of Engineers, Mohammed V University in Rabat, the Director of the Laboratory of Study and Research in Applied Mathematics (LERMA), and the Founding Member of Engineering for Smart and Sustainable Systems Research Center, E3S. His research interests include metaheuristics and nature inspired computing, optimization and uncertainties, finance, global, and stochastic optimization. Actually, he is the President of the Moroccan Society of Nature-Inspired Computing and Meta-Heuristics (METAH).

SALAH KAMEL received the international Ph.D. degree from Jaen University, Spain (Main), and Aalborg University, Denmark (Host), in January 2014. He is currently an Associate Professor with the Department of Electrical Engineering, Aswan University, Aswan, Egypt. He is also the Leader of the Advanced Power Systems Research Laboratory (APSR Lab), Power Systems Research Group, Aswan. His research interests include power system analysis and optimization, smart grid, and renewable energy systems.

• • •